Article

A Topological Analysis of Void Spaces in Tungstate Frameworks: Assessing Storage Properties for the Environmentally Important Guest Molecules and Ions: CO2, UO2, PuO2, U, Pu, Sr2+, Cs+, CH4, and H2

Jacqueline Manina Cole, Alisha Cramer, and Anita Zeidler

ACS Sustainable Chem. Eng., **Just Accepted Manuscript** • DOI: 10.1021/acssuschemeng.5b00369 • Publication Date (Web): 15 Jul 2015

A Topological Analysis of Void Spaces in Tungstate Frameworks: Assessing Storage Properties for the Environmentally Important Guest Molecules and Ions: CO_2, UO_2, PuO_2, U, Pu, Sr^{2+}, Cs^+, CH_4, and H_2

Jacqueline M. Cole,[a,b,c*] *Alisha J. Cramer,*[a] *Anita Zeidler*[c†]

Cavendish Laboratory, Department of Physics, University of Cambridge, J. J. Thomson Avenue, Cambridge, CB3 0HE. UK.

[b] Argonne National Laboratory, 9700 S Cass Avenue, Argonne, IL 60439. USA.

[c] Department of Chemistry, University of Cambridge, Lensfield Road, Cambridge, CB2 1EW. UK.

[†] Current address: Department of Physics, University of Bath, Bath, BA2 7AY. UK.

[*] Author for correspondence (E-mail: jmc61@cam.ac.uk)

Keywords: host-guest, tungstate, framework structure, energy fuel storage, CO_2 emissions, nuclear waste storage

Abstract

The identification of inorganic materials, which are able to encapsulate environmentally important small molecules or ions *via* host-guest interactions, is crucial for the design and development of next-generation energy sources and for storing environmental waste. Especially sought after are molecular sponges with the ability to incorporate CO_2, gas pollutants, or nuclear waste materials such as UO_2 and PuO_2 oxides or U, Pu, Sr^{2+} or Cs^{+} ions. Porous framework structures promise very attractive prospects for applications in environmental technologies, if they are able to incorporate CH_4 for biogas energy applications, or to store H_2, which is important for fuel cells e.g. in the automotive industry. All of these applications should benefit from the host being resistant to extreme conditions such as heat, nuclear radiation, rapid gas expansion, or wear and tear from heavy gas cycling. As inorganic tungstates are well known for their thermal stability, and their rigid open-framework networks, the potential of Na_2O-Al_2O_3-WO_3 and Na_2O-WO_3 phases for such applications was evaluated. To this end, all known experimentally-determined crystal structures with the stoichiometric formula $M_aM'_bW_cO_d$ (M = any element) are surveyed together with all corresponding theoretically calculated $Na_aAl_bW_cO_d$ and $Na_xW_yO_z$ structures that are statistically likely to form. Network descriptors that categorize these host structures are used to reveal topological patterns in the hosts, including the nature of porous cages which are able to accommodate a certain type of guest; this leads to the classification of preferential structure types for a given environmental storage application. Crystal structures of two new tungstates $NaAlW_2O_8$ (**1**) and $NaAlW_3O_{11}$ (**2**) and one updated structure determination of $Na_2W_2O_7$ (**3**) are also presented from in-house X-ray diffraction studies, and their potential merits for environmental applications are assessed against those of this larger

data-sourced survey. Overall, results show that tungstate structures with three-nodal topologies are most frequently able to accommodate CH_4 or H_2, while CO_2 appears to be captured by a wide range of nodal structure types. The computationally generated host structures appear systematically smaller than the experimentally determined structures. For the structures of 1 and 2, potential applications in nuclear waste storage seem feasible.

Introduction

For many years, porous materials have garnered considerable attention, owing to the wide range of applications that they potentially offer. The removal of pollutants from industrial waste,[1–3] the selective removal and storage of radioactive ions from nuclear waste,[4–7] and the storage of small molecules in alternative energy technologies[8–10] illustrate just a few of many possibilities. Currently, the focus of interest seems to be centered on organic-inorganic hybrid materials, generally known as metal-organic frameworks (MOFs), as these can be custom-tailored to a specific pore size.[3,8,11–17] Thus, MOFs have already demonstrated their potential as storage materials for alternative fuels such as CH_4 and H_2,[8,15,17–19] as CO_2 reservoirs for pollution-control measures,[3,20] or, more recently, for the potential uptake of volatile organic compounds.[21,22] The high level of success that MOFs have enjoyed sparked a search for other types of molecular architectures, which could be employed for similar tasks; this has led to the development of organic analogues of MOFs, of the so-called covalent organic frameworks (COFs).[23] Like MOFs, COFs have already proven their potential as storage materials for H_2, CH_4, CO_2, and N_2.[9,10] However, for applications involving harsher environmental pollutants, such as the storage of radioactive waste or volatile organic compounds, purely inorganic materials continue to dominate in practice.[1,2,4–7,24,25]

In order to determine the suitability of potential candidates for these types of applications, the void spaces in their crystalline solid-state frameworks should be examined initially. After all, only if the guest molecule can be accommodated in the host, are further considerations appropriate. In the ongoing search for usable materials, data mining of structure databases can provide a useful tool to identify potential candidates for the applications in hand. For example, a study on Li+ migration maps[26] examined the structure of channels within lithium-containing inorganic compounds, using Voronoi-Dirichlet partitioning that is implemented in the crystallographic topological analysis program TOPOS.[27] That study identified 277 out of 2171 crystal structures which contained suitable conduction channels; 26 of these structures, despite not being previously known as solid electrolytes, showed potential promise as ionic conductors.

We herein propose to employ Voronoi-Dirichlet partitioning to investigate the void space within cages of 3-dimensional tungstate-based extended framework structures in a similar way, i.e. by using topological net descriptors for comparisons in order to conduct a void space analysis for identifying possible host/guest combinations. To the best of our knowledge, this represents the first topological analysis of a large survey of tungstate structures, which are sourced from experimental and computational data. Experimental data emanate from the Inorganic Crystal Structure Database (ICSD) and from in-house crystallographic studies of three phases of Na_2O-WO_3. Computational data were obtained from a structure prediction approach, determining all structures containing Na^+, W^{6+} and O^{2-} ions with or without Al^{3+} ions, which are statistically likely to form based on ionic substitution considerations of known related structures. The topological nets and void volumes of all these crystal structures are determined and compared in order to assess their potential as hosts in host/guest media with environmental applications.

In the context of nuclear waste storage applications, the UO_2 and PuO_2 oxides, U and Pu ions of various oxidation states, and Sr^{2+} and Cs^{+} ions are explored as possible guests, out of the myriad of waste products found in nuclear waste. Waste from nuclear facilities, in the form of spent nuclear fuel, is found predominantly in the form of uranium or plutonium oxides.[28] Furthermore, current efforts, especially among tungstates, are largely focused on encapsulating radioactive waste via ion-exchange,[4–7,24,29] making the containment of U and Pu ions also important. Meanwhile, high activity fission product radionuclides Cs^{+} and Sr^{2+} provide an additional focus for storage development. Within waste streams from nuclear reactors, ^{137}Cs and ^{90}Sr generate most of the thermal heat found in high level waste, and combined with their relatively short half-lives (<50 years), processing these two elements separately from the rest of the waste stream is both practical and beneficial.[30] In the context of environmental waste associated with climate change, the encapsulation of CO_2 is evaluated with a view to offset carbon emissions. Meanwhile, the possible inclusion of CH_4 and H_2 molecules is considered for alternative energy storage applications, which stand to deter carbon emissions.

The diverse origins of the obtained data also provide the opportunity to make a general comparison of experimentally determined against theoretically calculated structures for this family of inorganic materials; and to establish a relative ranking of the likely use of three in-house characterized subject materials $Na_aAl_bW_cO_d$ (a =1,2; b = 0,1; c = 2,3; d = 7,8,11) within this representative set of all statistically conceivable tungstate framework structures.

The overarching workflow associated with this topologically-generated data-mining study that pair-wise matches host-guest volumes is illustrated in Figure 1.

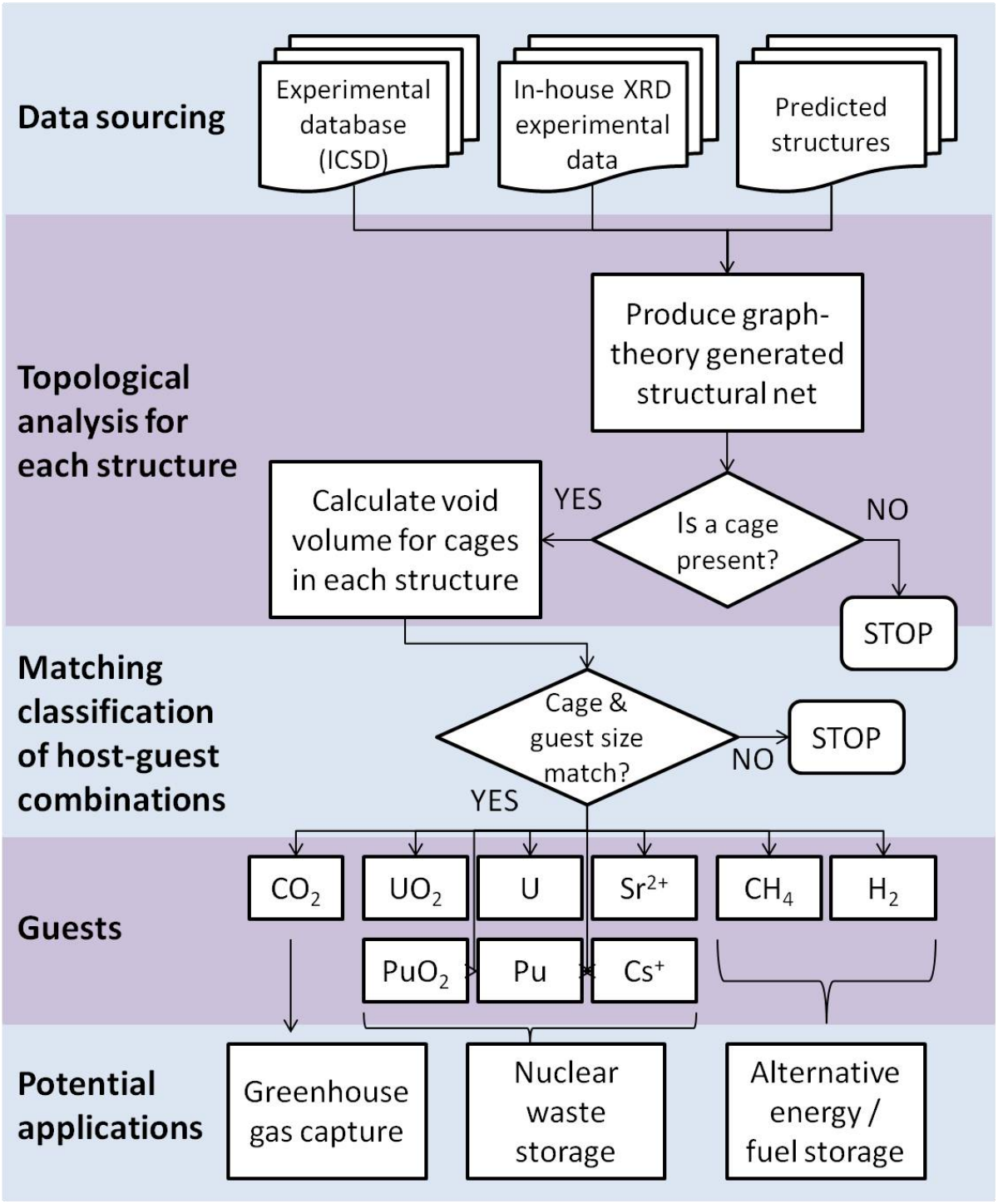

Figure 1. The overarching workflow for suiting host-guest pairs in tungstate-based structures with porous cages for guest inclusion.

Experimental and Computational Methods

Experimentally-derived crystal structure data of tungstate framework structures. Data for all 378 previously-reported crystal structures of ternary and quaternary tungstates of the general formulae $M_aW_yO_z$ or $M1_aM2_bW_yO_z$ (M, M1, M2 = any element) were extracted from the Inorganic Crystal Structure Database (ICSD). 284 of this total, which displayed structural frameworks that produce cages, were taken forward for full data analysis. Search parameter filters within the ICSD restricted structures to those containing W, O, and either 3 or 4 total element species. From the results, disordered structures, and those with partial occupancy in one or more of the atomic sites were manually excluded. The remaining list of structures was further refined by manually removing duplicates (structures with the same chemical formula, and spacegroup); among duplicate structures, those with the lowest R1 factor were kept.

In-house provision of crystal structure data: sample preparation and characterization of three Na2O-Al2O3-WO3 and Na2O-WO3 phases. Samples were prepared as previously described elsewhere.[31] The crystal structures of two new compounds $NaAlW_2O_8$ (**1**) and NaAlW3O11 (**2**) were determined by single crystal X-ray diffraction. Furthermore, the crystal structure of Na2W2O7 (**3**), was determined at low temperature (T = 180(2) K), affording an improved structural model on the previously reported room-temperature structure.[32]

Suitable single crystals were mounted onto glass fibers using perfluoropolyether oil. Diffraction data for (**1**) were collected on a Nonius Kappa CCD diffractometer, equipped with a monochromatic Mo-Kα (λ = 0.71073 Å) X-ray source and an Oxford Cryosystems Cryostream open-flow N_2 cooling device. Cell parameters were refined against data from all regions of reciprocal space using HKLScalepack.[33] Data reduction employed HKLDenzo and Scalepack,[33] while data sets were corrected for Lorentz and polarisation effects, as well

as for absorption using SORTAV.[34] Diffraction data for (**2**) and (**3**) were collected on a Rigaku Saturn 724+ CCD diffractometer, equipped with a monochromatic Mo-Kα (λ = 0.71073 Å) X-ray source, SHINE Optics, and an Oxford Cryosystems CryostreamPlus open-flow N_2 cooling device. Cell refinement, data collection, and data reduction were carried out with Rigaku CrystalClear-SM Expert 2.0 software,[35] whereas absorption correction was implemented using ABSCOR.[36]

All structures were solved with direct methods and refined by full-matrix least squares methods on F2 using SHELXL-97.[37] Full details for crystal, data collection and refinement parameters are provided in the Supporting Information.

A few specific technical notes about the structure solution and refinement of (**1**)-(**3**) are worth mentioning. Owing to its pseudo-orthorhombic unit cell, the structure of (**1**) displays a small, but nevertheless distinct, pseudo-merohedral twin component, resulting in a fractional twin contribution of 0.16(3)%. Compound (**2**) displays significant structural disorder, to the extent that its elemental and stoichiometric composition needed verification from energy-dispersive X-ray (EDX) analysis to aid crystal structure determination. The EDX experiment employed a Zeiss Cross Beam scanning electron microscope, which afforded the following elemental proportions: Na = 5.47%; Al = 5.13%; W = 15.54%; O = 65.62%. A residual 8.34% arising from a contribution of carbon was attributed to surface contamination. These results were particularly important in checking that the compound contained Al, rather than Cr, which could have substituted Al as a reaction contaminant. The structure of (**3**) matches the previously determined crystal structure of this material,[32] albeit with improved refinement statistics and different thermal parameters owing to the low-temperature data collection nature of this new study.

Theoretically calculated predictions for tungstate structures. All hypothetically possible crystal structures containing any statistically conceivable combination of W, P, Al and O ions were generated computationally by using previously described methods.[38] The possibility of individual crystal structures was based on the statistical probability for existing structural motifs in the Inorganic Crystal Structure Database (ICSD) to be transmuted into tungstates via ionic substitution. The probability of ionic substitution was determined via a reference pair correlation matrix of various ion combinations, where each matrix element, gAB, represents the probability of ionic substitution between a given pair of ions A and B. This probability has been pre-calculated by enumerating the relative number of crystal structure examples in the ICSD, which differ only in the ions A and B. This method accordingly assesses the relative ease by which a given ion can fit into the crystallographically equivalent site of another ion. Values for gAB were therefore derived from a pre-trained reference library of structural homologues of A and B. While this was not part of the probabilistic calculation, it is hardly surprising that two ions of similar size, chemical properties (e.g. from the same group in the periodic table), and/or identical charge tend to have higher gAB values, since substitution for each proceeds more readily. For example, when A = W^{6+}, the highest gAB value was obtained for B = Mo^{6+}, whereas when A = Al^{3+}, large gAB values were obtained for B = Cr^{3+}, Fe^{3+}, In^{3+}, or Ga^{3+}.

Only charge-balanced crystal structures, and those not already in the ICSD, were considered in the theoretical structure prediction results. In total, 196 hypothetical tungstate structures of the general formula $Na_mW_nAl_oO_p$ were generated computationally. 43 of these calculated structures were taken forward for full void-space analysis since only these produced cages, which are of course necessary for hosting guest molecules or ions.

Topological Analysis

TOPOS methods. All selected tungstate structures were assessed for their potential for hosting the subject guest molecules and ions, using the crystallographic topological analysis program package, TOPOS 4.0 Professional.[27] This enabled the topological classification of each tungstate structure, and the determination and analysis of the void space residing within its framework.

This analysis was accomplished by first defining the topological net of each structure using the ADS module in TOPOS. Such nets were identified using graph theory to calculate a map of the circuits contained therein by viewing all atoms as nodes, and all bonds as edges, thereby ascertaining the geometrical patterns in the crystal structure. These nets were then categorized as n-nodal in the presence of n different kinds of inequivalent vertices in the net. The net may contain tiles, defined as generalized polyhedra (cages) which have at least two edges incident upon each vertex and two faces incident upon each edge.[39,40] These tiles are described according to how many faces a given tile possesses with each face being defined by its m-membered rings. This nodal/tiling topological representation is illustrated in Figure 2, using the example of (**1**). The full classification of a net is based on several conventional descriptors, which may be used to search the TOPOS Topological Database (TTD) for the topological type of the net (for a full explanation and list of these descriptors see [41,42]).

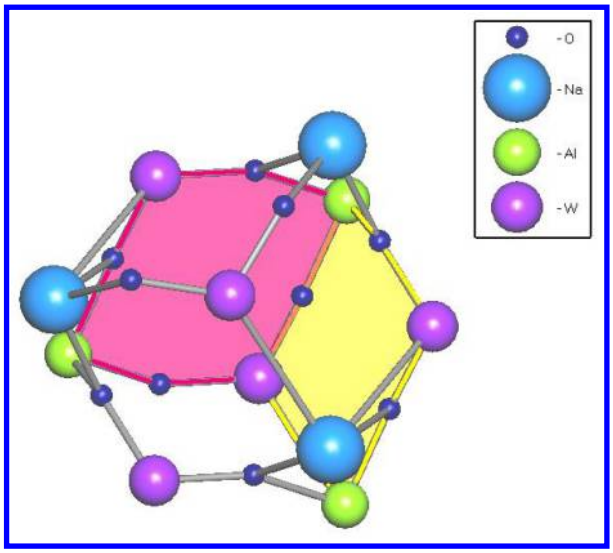

Figure 2. A 22/11 net using (**1**) as the example: $[3^2.4^3.6.7^2.8^3]$ tile, whereby 22/11 denominates the total number of nodes/tiles; $[3^2.4^3.6.7^2.8^3]$ indicates the presence of 2 faces consisting of 3-membered rings, 3 faces consisting of 4-membered rings, 1 face consisting of a 6-membered ring, 2 faces consisting of 7-membered rings (e.g. yellow plane), and 3 faces consisting of 8-membered rings (e.g. pink plane).

Void space analysis was then accomplished via a two-step process: the determination of all cages found within each structure, prior to calculating the void space volume within each cage using Voronoi-Dirichlet polyhedra (VDP). Thus, a comparison basis for the cavity volumes in each structure was established in the first step. Cages can be found from the net topology, and were determined using the ADS module in TOPOS. For three-dimensional periodic framework structures, the circuits formed by the atoms and bonds can be combined to form generalized polyhedra that are topologically equivalent to spheres. For an in-depth discussion of cages and tiling, see [39,43].

The second step of void-space analysis comprises the calculation of a Voroni-Dirichlet partition of the crystal space for each cage, using the Dirichlet module in TOPOS to construct the VDP for all independent framework atoms. From this partition, the location and size of voids were obtained by placing a node at the intersection of four or more VDP vertices. Subsequently, the Voroni-Dirichlet partition was reconstructed taking the void nodes into account, which resulted in a map of the void space of the structure. In order to analyze the cavity size within individual cages, the cages were isolated and void nodes were generated from the atoms forming the cage. Subsequently, VDP were generated for these void nodes, from which their volumes were calculated.

Guest volume determination. The intrinsic volumes of the guest molecules or ions were estimated in three different ways. For individual ions (U, Pu, Cs^{+}, Sr^{2+}), radii of 1.75 Å, 1.75 Å, 2.60 Å, and 2.00 Å, respectively, were obtained from the Slater radii[44] database in TOPOS. Subsequently, these radii where employed to calculate spherical volumes. The volumes of the UO_2 and PuO_2 oxides were extracted from their previously reported experimentally-determined crystal structures, as sourced from the ICSD. Owing to the three dimensional frameworks formed by UO_2 and PuO_2 crystal structures, volume determination of discrete molecules was unfeasible. Hence, the volumes of a single U or Pu, and the eight valence-bonded oxygens for each were determined for chosen samples of UO_2[45] and PuO_2,[46] respectively.

Volumes for small guest molecules, such as CO_2, CH_4, and H_2 were established based on previously published kinetic diameters (3.3 Å, 3.8 Å, and 2.89 Å, respectively), from which spherical volumes were calculated. As the kinetic diameter represents only the smallest dimension of a given molecule, the calculated spherical volumes are necessarily the smallest possible volume for that molecule, and there is no consideration of the shape of the molecule in this calculation. This is acceptable as long as an upper bound of guest volumes within a cage can be set to provide the necessary latitude to allow for the molecule size to be greater in its other dimensions.

The resulting volumes for all guest molecules and ions were rounded up to the nearest whole integer, in order to establish the lowest bound of the desired cage size. An upper bound was set 4 $Å^3$ above this lower bound, which should allow the guest some spatial flexibility, without allowing more than one guest within a single cage. An exception to this is H_2, where a maximum of two molecules may fit in a cage at the upper limit.

Results and Discussion

New Crystal Structures

$NaAlW_2O_8$ (1). The W-Al network in (**1**) consists of 4-membered rings with alternating octahedrally-coordinated Al and tetrahedrally-coordinated W atoms, whereby Na atoms occupy the space between rings (Figure 3 (left)). One might naturally suppose that the framework of (**1**) would be isostructural to the previously reported $MM'W_2O_8$ (M, M' = metal) crystal structures, $NaCrW_2O_8$ and $NaInW_2O_8$, which form layers of polyhedra in the order Na, W, In/Cr, W, Na yielding a 2-nodal net of the α-PbO_2 topological type.[47] However, it is not; instead, (**1**) turns out to be isomorphic with the molybdate compound, $NaAlMo_2O_8$,[48] manifesting coordination polyhedra that form a 6-nodal topological net.

All atoms in the structural framework of (**1**) lie on general positions with the exception of the Al, which is located on an inversion centre. The observed W···O bond lengths range from 1.743 (5) - 1.806 (4) Å, whereas the Al···O bond lengths range from 1.874 (4) - 1.891 (4) Å, and the Na···O bond lengths span a range from 2.367 (4) - 2.924 (4) Å.

$NaAlW_3O_{11}$ (2). (**2**) features two tetrahedral and one octahedrally coordinated W, as well as one octahedrally-coordinated Al, forming the main part of the network, with Na atoms occupying sites inside the framework. The W-Al network adopts a (3,6)-coordinated 2-nodal net which corresponds to a standard toplogical type, 3,6T36. This network consists of 4-membered rings of alternating octahedrally-coordinated W and Al, which are connected *via* their apexes to 4-membered rings of alternating octahedrally-coordinated Al and tetrahedrally-coordinated W ions (Figure 3 (middle)). Inclusion of the Na ions results in the formation of a 9-nodal net.

$Na_2W_2O_7$ (3). In contrast to (**1**) and (**2**), (**3**) lacks any Al ions, and so the coordination sites of its structure contain exclusively octa- and tetrahedrally coordinated W ions (Figure 3 (right)). Topologically, this can be classified as a 9-nodal net. The W network contains long chains of octahedrally-coordinated W, wherein the tetrahedrally-coordinated W ions adopt alternating positions on both sides of the chain. The Na ions occupy coordination sites between these chains, coordinating to the terminal oxygens of the tetra- and octahedrally-coordinated W ions.

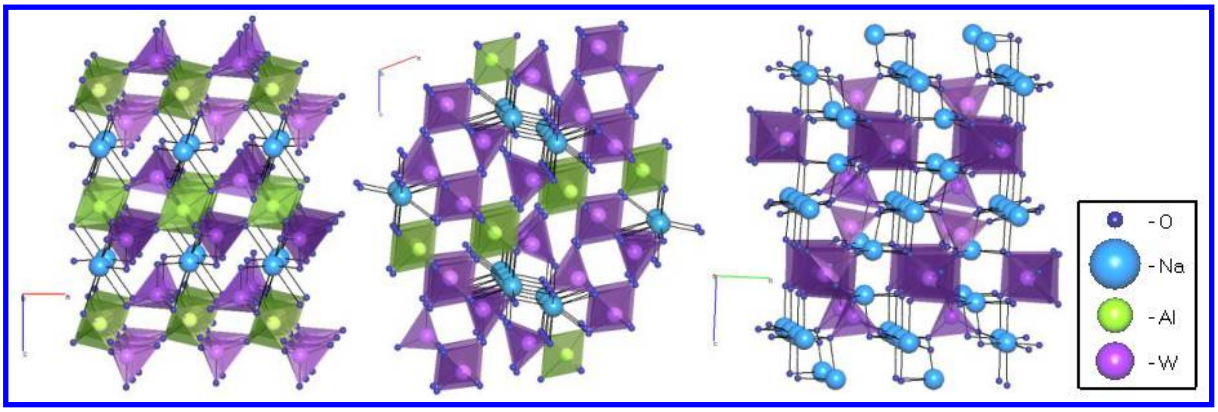

Figure 3. The crystal structures of (**1**) and (**2**) viewed down the b-axis (left and middle); and (**3**) viewed down the a-axis (right).

Guest/host comparisons for environmental applications. In total, 577 crystal structures of tungstate-based extended frameworks were surveyed for their prospects as host materials for the environmentally important guest molecules or ions: CO_2, UO_2, PuO_2, U, Pu, Sr^{2+}, Cs^+, CH_4, and H_2. 196 were hypothetical crystal structures generated from computational predictions, while the other 381 were sourced from (378) previously reported or (3) in-house data from diffraction experiments. Of these, 284 previously reported crystal structures, 43 hypothetical structures, and the three in-house determined structures produced topological tilings; the ten largest cages in these 331 tilings were subsequently identified and their corresponding void volumes calculated (see Supporting Information). Possible guest-host

matches were then assessed by comparing these void space volumes of the framework structures against the size of each subject guest molecule or ion.

CO_2 capture. The optimal cavity size for the incorporation of CO_2 was determined using its kinetic diameter of 3.3 Å,[49] providing a target volume of 19 – 23 $Å^3$. The structural analysis identified 52 previously reported experimentally-determined crystal structures containing 60 cages with appropriate void space volumes. Of these, 47 structures had one suitable cage volume per structure; the remaining 5 structures contained two or more suitable cages (hereafter designated as 'multiple cages') per structure. The subsequent breakdown of all suitable cages by type found that 16 cages suited for hosting a guest were found to be the largest (primary, 1°) cage formed by the structure, whereas in 17 of the cages it was the secondary (2°) cage with suitable void space, and 27 cages of interest were tertiary (3°) or higher ($3°^+$). Furthermore, five of the compounds contained at least two cages suitable for CO_2 storage. Among the calculated structures, a total of 13 structures were found to contain 21 suitable cages (1 x 1°; 3 x 2°; 17 x $3°^+$), with seven of the structures exhibiting multiple cages. None of the in-house experimentally-determined crystal structures (1)-(3) were found to contain cages suitable for CO_2 containment. Figure 4 summarizes these statistics, while representative example structures from the most common (5- and 6-nodal) nets that demonstrate capacity to host CO_2 are displayed in Figure 5.

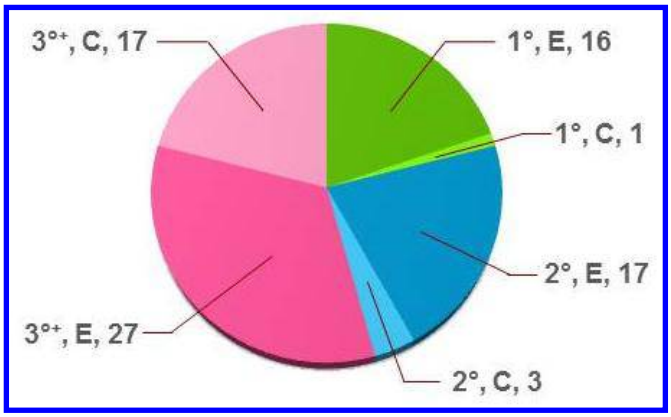

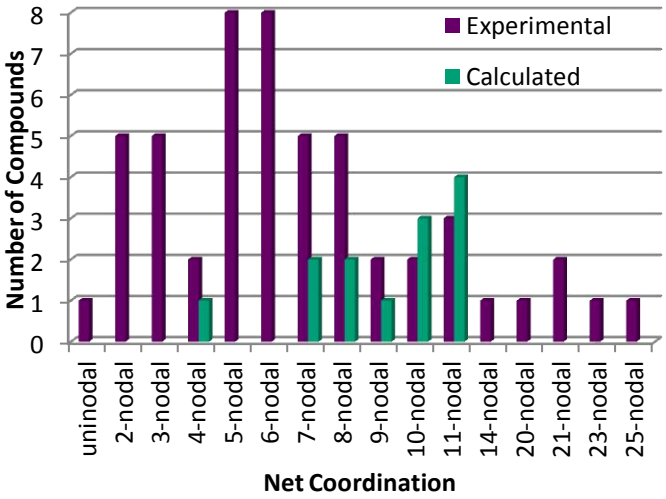

Compound	Cage attribute	Ref. [ICSD -paper]
$Li(NbWO_6)$	E, 1°	45799 – [50]
$Li(TaWO_6)$	E, 1°	45800 – [50]
$Na(NbWO_6)$	E, 1°	45802 – [50]
$Na(TaWO_6)$	E, 1°	45803 – [50]
$Na(VWO_6)$	E, 1°	174133 – [51]
$BiNdWO_6$	E, 1°	416789 - [52]
$KEu(WO_4)_2$	E, 1°	173634 - [53]
Ba_2SrWO_6	E, 1°	246115 - [54]
$Gd_3(BWO_9)$	E, 1°	250417 - [55]
$Nd_3(BWO_9)$	E, 1°	250415 - [55]
$Sm_3(BWO_9)$	E, 1°	250416 - [55]
$Pr_3(BWO_9)$	E, 1°	250414 - [55]
$Ba_{11}(W_4O_{23})$	E, 1°	418207 - [56]
$Li_2Zn_2(W_2O_9)$	E, 1°	160509 - [57]
$La_2(WO_4)(Te_3O_7)_2$	E, 1°	249538 - [58]
Ba_2SrWO_6	E, 1°- 3°	246108 - [54]
$Gd(WO_4)Cl$	E, 2°	35292 - [59]
Ba_2SrWO_6	E, 2°	246113 - [54]
$Eu_2(MoW_2O_{12})$	E, 2°	155946 - [60]
$Na_4Th(WO_4)_4$	E, 2°	422185 - [61]
$Na_5Lu(WO_4)_4$	E, 2°	200930 - [62]
$Na_5Tb(WO_4)_4$	E, 2°	20426 - [63]
$Na_5La(WO_4)_4$	E, 2°	20427 - [63]
$Sr_8Cu(WO_6)_3$	E, 2°	183646 - [64]
$Hg(WO_4)$	E, 2°	169670 - [65]
$K(W_3O_9)$	E, 2°	100228 - [66]
$K_2W_4O_{13}$	E, 2°	2412 - [67]
$Eu_2(Mo_2WO_{12})$	E, 2°	155945 - [60]
$Hg_2(WO_4)$	E, 2°	90085 - [68]
Ba_2WO_5	E, 2°	62489 - [69]
$K_2(WO_4)$	E, 2°	150840 - [70]
$Li_2(W_2O_7)$	E, 2°- 3°	1897 - [71]
$ErBi(W_2O_9)$	E, 3°	183443 - [72]
$EuBi(W_2O_9)$	E, 3°	183444 - [72]
$SmBi(W_2O_9)$	E, 3°	183445 - [72]
$Na_3F(WO_4)$	E, 3°	417289 - [73]
$Na_5Y(WO_4)_4$	E, 3°	417143 - [74]
UW_3O_{11}	E, 3°	81983 - [75]
Cu_2WO_4	E, 3°	62058 - [76]
$Pb_3(WO_5)Cl_2$	E, 3°	89833 - [77]
$CuDy(WO_4)_2$	E, 4°	73749 - [78]
$CuEr(WO_4)_2$	E, 4°	73747 - [78]
$CuLa(W_2O_8)$	E, 4°	68614 - [79]
$Tl_2(WO_4)$	E, 4°	8212 - [80]
$Ce_{10}W_{22}O_{81}$	E, 4°- 5°	260095 - [81]
$Cu_2(WO_4)$	E, 5°	202669 - [82]
$FeCe(WO_4)(W_2O_8)$	E, 6°	401919 - [83]
$K_2Nb_{10}W_7O_{47}$	E, 6°	62130 - [84]
$Al_2(WO_4)_3$	E, 6°	73878 - [85]
$Al_2(WO_4)_3$	E, 6°	90936 - [86]
$Ag_{26}I_{18}(WO_4)_4$	E, 6°- 9°	56852 - [87]
$Al_2(WO_4)_3$	E, 9°- 10°	56827 - [85]
$Na_2W_2O_7$	C, 1°	
Na_2WO_4	C, 2°	
Na_2WO_4	C, 2°- 4°	
$Na_2W_2O_7$	C, 2°- 4°	
$Na_2W_2O_7$	C, 3°	
$Na_2W_2O_7$	C, 3°- 4°	
Na_2WO_4	C, 4°	
$Na_2W_2O_7$	C, 4°	
$NaAlW_2O_8$	C, 4°	
$NaAlW_2O_8$	C, 4°	
$NaAlW_2O_8$	C, 4°- 5°	
$Na_2Al_2WO_7$	C, 4°- 5°	
$Na_2W_2O_7$	C, 7°- 8°	

Figure 4. (left) Distribution of cage types (1°, 2°, $3^{\circ+}$) of host structures comprising n-nodal nets that can incorporate CO_2, according to their frequency observed in experimental (E) and calculated (C) crystal structures; (right) a list of their associated compound identifiers (ICSD number and reference citation).

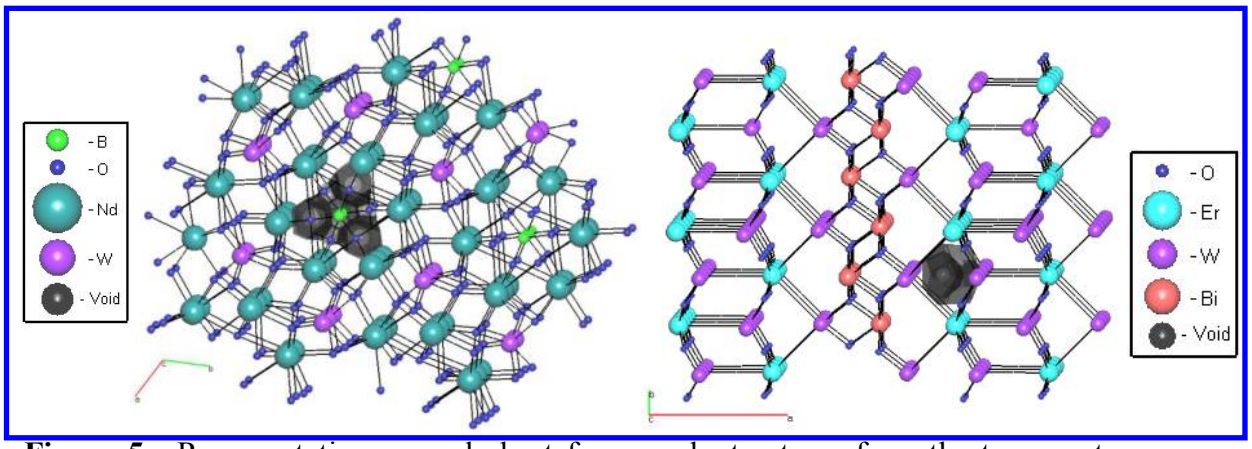

Figure 5. Representative example host framework structures from the two most common types of n-nodal nets whose cages have suitable void space volumes (black/grey) to accommodate CO_2 molecules: 5-nodal (left; $Nd_3(BWO_9)$ [ICSD ref. 250415 – [55]]) and 6-nodal (right; $ErBi(W_2O_9)$ [ICSD ref. 183443 – [72]]).

Nuclear waste storage.

UO_2. The potential inclusion of UO_2 was examined on the basis of the TOPOS-generated VDP volume for a single cube of 8-coordinated U from the UO_2 crystal structure (ICSD reference no. 246851 – [45]; space group *Fm-3m*; unit cell a = 5.468Å). This produced a void-space volume of 63.09 $Å^3$ which gave a targeted void space volume of 64 – 68 $Å^3$. This range identified only two suitable cages within previously reported structures, one within predicted structures, and two within the in-house structures ((**1**) and (**2**)), as seen in Figure 6. All structures contained only 1° cages. With such a limited sampling, there is no net type that is more common than any other for hosting UO_2. As such, (**1**) will serve as the representative example structure with a 6-nodal net, shown in Figure 7.

Compound	Cage attribute	Ref. [ICSD - paper]

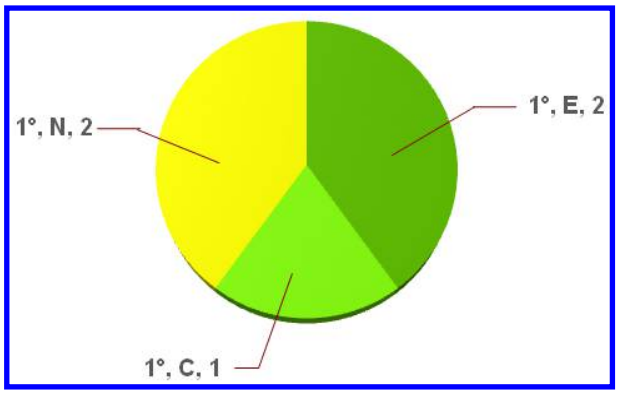

$FeCe(WO_4)(W_2O_8)$	E, 1°	401919 - [83]
$Zr(WO_4)_2$	E, 1°	262062 - [88]
$NaAlW_2O_8$	N, 1°	This work – [(**1**)]
$NaAlW_3O_{11}$	N, 1°	This work – [(**2**)]
$Na_2W_2O_7$	C, 1°	

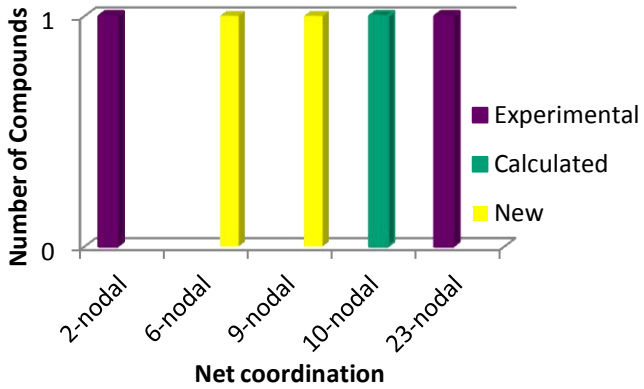

Figure 6. (left) Distribution of cage types (1°) of host structures comprising n-nodal nets that can incorporate UO_2, according to their frequency observed in previously reported (E) or newly-determined (N) experimental and calculated (C) crystal structures; (right) a list of their associated compound identifiers (ICSD number and reference citation).

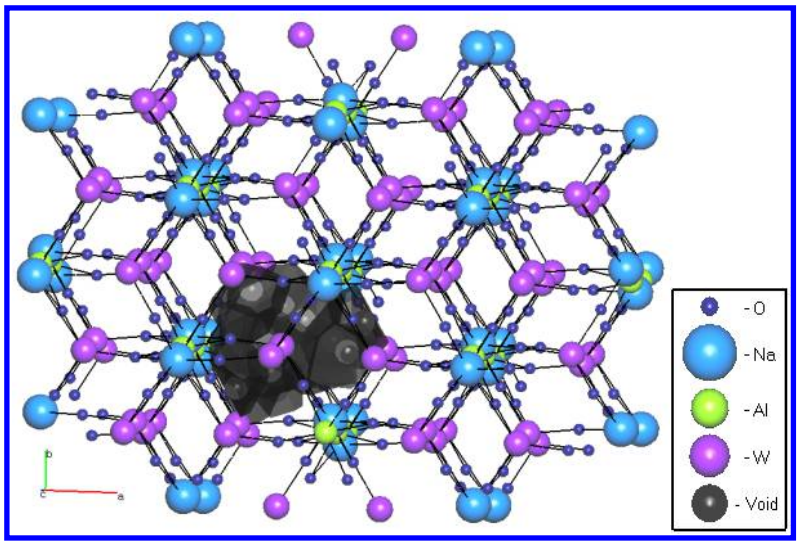

Figure 7. A representative example of a crystal structure (of $NaAlW_2O_8$ [this work (**1**)]) bearing a (n = 6) n-nodal net that contains cages with suitable void space volumes (black/grey) to accommodate UO_2.

PuO_2. Determination of the PuO_2 volume followed the same general pattern as for UO_2. The VDP volume of a single cube of 8-coordinated Pu was obtained from TOPOS using the PuO_2 crystal structure (ICSD reference no. 55456 – [46], space group Fm-3m, unit cell a = 5.3982 Å). This afforded a target void-space volume range of 61 – 65 $Å^3$. The topological analysis identified eight suitable cages amongst seven previously reported crystal structures: 6 x 1°; 2 x 2°, with one structure containing both 1° and 2° cages of a suitable size; a 3° cage in one predicted structure, and a 1° cage in the new structure, (**2**). Figure 8 summarizes these statistics. Figure 9 provides a representative example of a tungstate-based framework structure belonging to the most common type of n-nodal net (n = 9) that bears a cage suitable for PuO_2 containment.

Compound	Cage attribute	Ref. [ICSD -paper]
$Zr(WO_4)_2$	E, 1°	262062 - [88]
$Ba_3WO_5Cl_2$	E, 1°	63518 - [89]
$Er_2(WO_6)$	E, 1°	62885 - [90]
$Y_2(WO_6)$	E, 1°	65811 - [91]
Gd_2WO_6	E, 1°	62888 - [92]
$FeCe(WO_4)(W_2O_8)$	E, 1° - 2°	401919 - [83]
$(Na_2WO_4)(H_2O)_2$	E, 2°	240882 - [93]
$NaAlW_3O_{11}$	N, 1°	This work – [(**2**)]
$Na_2W_4O_{13}$	C, 3°	

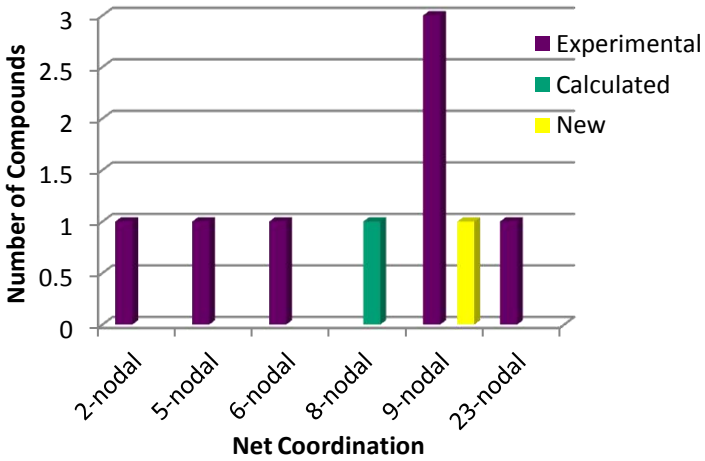

Figure 8. (left) Distribution of cage types (1°, 2°, 3°) of host structures comprising n-nodal nets that can incorporate PuO_2, according to their frequency observed in previously reported (E) or newly-determined (N) experimental and calculated (C) crystal structures; (right) a list of their associated compound identifiers (ICSD number and reference citation).

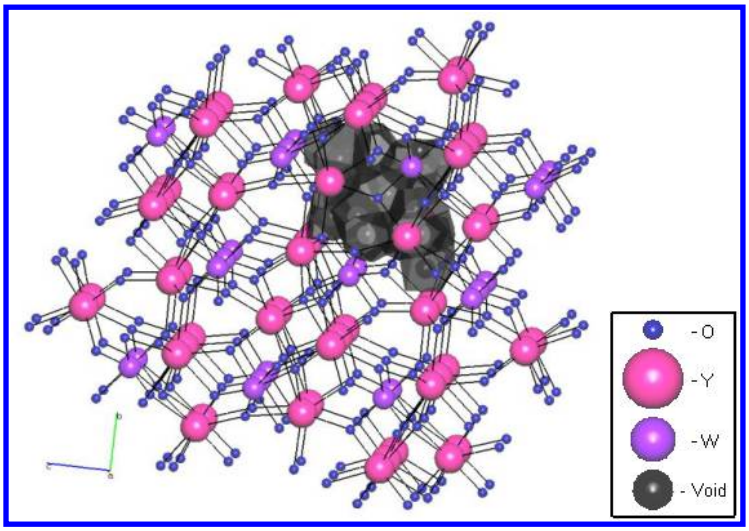

Figure 9. A representative example of a crystal structure (of $Y_2(WO_6)$ [ICSD ref. 65811 – [91]]) bearing the most common (n = 9) n-nodal net that contains cages with suitable void space volumes (black/grey) to accommodate PuO_2.

U or Pu ions. Although it would be more accurate to investigate ions, differences in reactor type, reprocessing, and waste management techniques can result in different states of a given ion within the waste material. In natural water-rock systems, Pu has four oxidation states (3^+, 4^+, 5^+, 6^+), while U can often be found as U^{4+} or U^{6+};[94] as such, it was decided to use the atomic radii for these elements since this represents the largest volume that would potentially be necessary for encapsulation. U and Pu atoms presented the same Slater radii[44] listings in TOPOS, and so were considered together in terms of finding suitable host structures to contain them. The associated target void-space volumes were 23-27 $Å^3$. This resulted in the selection of 45 previously reported crystal structures that feature 68 suitable cages (11 x 1°; 18 x 2°; 39 x $3°^+$; 13 x multiple cages); 13 predicted structures (2 x 1°; 6 x 2°; 6 x $3°^+$) one of which contains both a 2° and 3° cage; and one newly-determined crystal structure, ((**3**), bearing a 2° cage). Figure 10 displays these results. A representative example structure, bearing the most common type of n-nodal net (n = 3) whose cages appear to be able to host U or Pu ions, is presented in Figure 11.

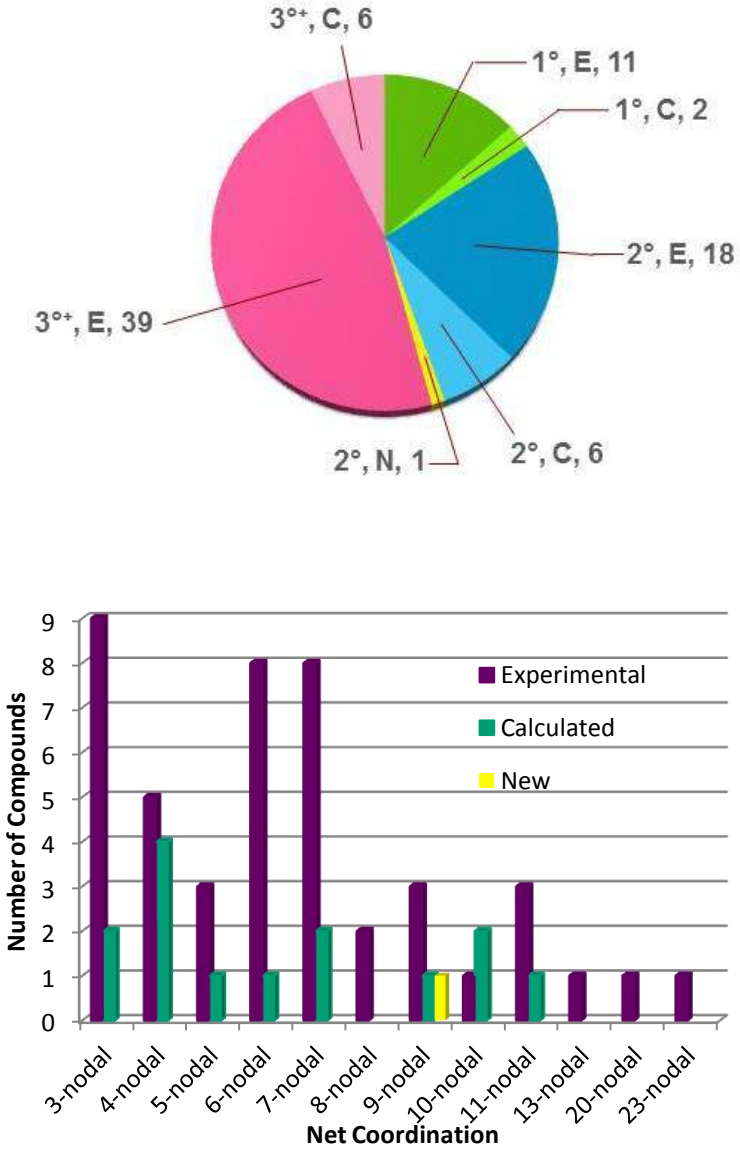

Compound	Cage attribute	Ref. [ICSD - paper]
$KLu(WO_4)_2$	E, 1°	172510 - [95]
$KYb(WO_4)_2$	E, 1°	280877 - [96]
$KEr(WO_4)_2$	E, 1°	157832 - [97]
$KY(WO_4)_2$	E, 1°	411285 - [98]
$KHo(WO_4)_2$	E, 1°	182626 - [99]
$Sr_2(CuWO_6)$	E, 1°	99303 - [100]
$Li_2Cu(WO_4)2$	E, 1°	92854 - [101]
$Li_2Ni(WO_4)_2$	E, 1°	92853 - [101]
$Li_2Co(WO_4)_2$	E, 1°	92852 - [101]
$Ce_{10}W_{22}O_{81}$	E, 1° - 3°	260095 - [81]
Bi_2WO_6	E, 1° - 3°	171328 - [102]
$Dy_2(WO_4)_3$	E, 2°	98102 - [103]
$Eu_2(WO_4)_3$	E, 2°	15877 - [104]
$Pb_3(WO_5)Cl_2$	E, 2°	89833 - [77]
$Pr_3(WO_6)Cl_3$	E, 2°	20626 - [105]
$La_3WO_6Cl_3$	E, 2°	35595 - [106]
$Rb_{12}(Nb_{30}W_3O_{90})$	E, 2°	1505 - [107]
$LiY(W_2O_8)$	E, 2°	156989 - [108]
$ErBi(W_2O_9)$	E, 2°	183443 - [72]
$EuBi(W_2O_9)$	E, 2°	183444 - [72]
$SmBi(W_2O_9)$	E, 2°	183445 - [72]
$Ca_4(Al_6O_{12})(WO_4)$	E, 2°	28481 - [109]
$Na_2(W_2O_7)$	E, 2°	1883 - [32]
$Sr_4(Al_6O_{12})(WO_4)$	E, 2°	28483 - [109]
UW_3O_{11}	E, 2°	81983 - [75]
$Ba_3WO_5Cl_2$	E, 2° - 3°	63518 - [89]
$CuSm(W_2O_8)$	E, 2° - 3°	68615 - [79]
$CuGd(W_2O_8)$	E, 3°	75006 - [110]
$LiPr(WO_4)_2$	E, 3°	200520 - [111]
$CuDy_5(WO_4)_8$	E, 3°	380067 - [112]
$Tl_2(WO_4)$	E, 3°	8212 - [80]
$Rb_2(WO_4)$	E, 3°	183200 - [113]
$Rb(NbW_2O_9)$	E, 3°	246143 - [114]
$Al_2(WO_4)_3$	E, 3° - 5°	73878 - [85]
$Al_2(WO_4)_3$	E, 3° - 5°	90936 - [86]
$FeCe(WO_4)(W_2O_8)$	E, 4° - 5°	401919 - [83]
$U(WO_4)$	E, 4° - 5°	2285 - [115]
$Al_2(WO_4)_3$	E, 4° - 8°	56827 - [85]
$Li_2(WO_4)$	E, 5° - 6°	160721 - [116]
$Li_2(WO_4)$	E, 5° - 6°	15395 - [117]
$Sc_2(WO_4)_3$	E, 6°	28467 - [118]
$In_2(WO_4)_3$	E, 6°	99606 - [119]
$Ba_2P_8W_{32}O_{112}$	E, 7° - 9°	202484 - [120]
$Al_2(WO_4)_3$	E, 8° - 10°	73879 - [85]
$(Na_2WO_4)(H_2O)_2$	E, 9°	240882 - [93]
$Na_2W_2O_7$	N, 2°	This work – [(**3**)]
Na_2WO_4	C, 1°	
Na_2WO_4	C, 1°	
Na_4WO_5	C, 2°	
Na_2WO_4	C, 2°	
$Na_2W_2O_7$	C, 2°	
$Na_2W_2O_7$	C, 2°	
$Na_2W_2O_7$	C, 2°	
$Na_2Al_2WO_7$	C, 2° - 3°	
Na_2WO_4	C, 3°	
$Na_2W_2O_7$	C, 3°	
$Na_2W_2O_7$	C, 3°	
$NaAlW_2O8$	C, 3°	
$Na_2W_2O_7$	C, 8°	

Figure 10. (left) Distribution of cage types (1°, 2°, 3°$^+$) of host structures comprising n-nodal nets that can incorporate U or Pu ions, according to their frequency observed in previously reported (E) or newly-determined (N) experimental and calculated (C) crystal structures; (right) a list of their associated compound identifiers (ICSD number and reference citation).

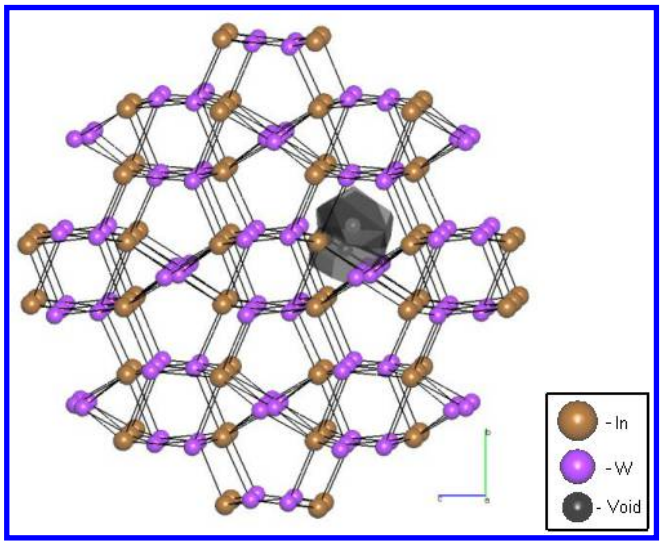

Figure 11. A representative example of a crystal structure (of $In_2(WO_4)_3$ [ICSD ref. 99606 – [119]]) featuring the most common (n = 3) n-nodal net that bears cages with suitable void space volumes (black/grey) to contain U or Pu ions.

Cs^+ ions. The occupational volume for Cs^+ ions was also obtained from the Slater radius[44] parameter in TOPOS, resulting in a target void-space volume of 74 – 78 $Å^3$. For this range, suitable cages in four previously reported (3 x 1°; 1 x 2°) and four predicted (3 x 1°; 1 x 2°) structures were identified (Figure 12). Figure 13 illustrates a representative example of a host structure bearing the most common n-nodal set (n = 6) that features suitable cages to contain Cs^+ ions.

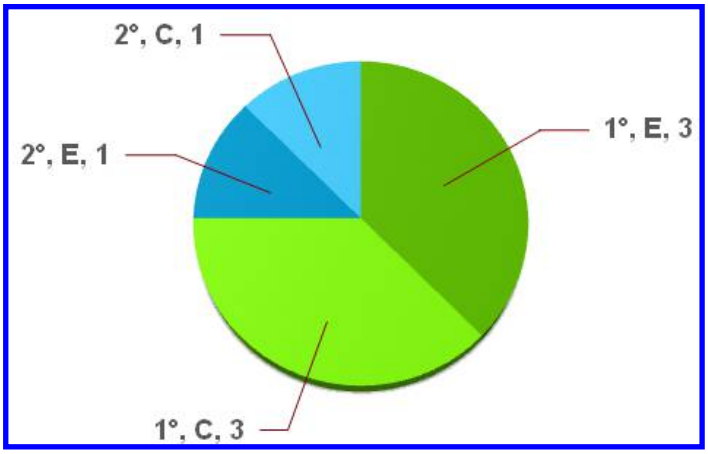

Compound	Cage attribute	Ref. [ICSD - paper]
$Gd(WO_4)Cl$	E, 1°	35292 - [59]
$Ca_2Ni(WO_6)$	E, 1°	160109 - [121]
$Li_2(WO_4)$	E, 1°	10479 - [122]
$Ca_8(Al_{12}O_{24})(WO_4)_2$	E, 2°	71806 - [123]
$Na_2W_2O_7$	C, 1°	
$NaAlW_2O_8$	C, 1°	
$NaAlW_2O_8$	C, 1°	
$NaAlW_2O_8$	C, 2°	

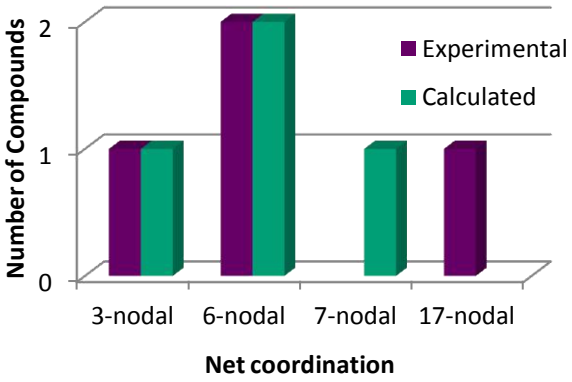

Figure 12. (left) Distribution of cage types (1°, 2°) of host structures comprising n-nodal nets that can incorporate Cs^+ ions, according to their frequency observed in experimental (E) and calculated (C) crystal structures; (right) a list of their associated compound identifiers (ICSD number and reference citation).

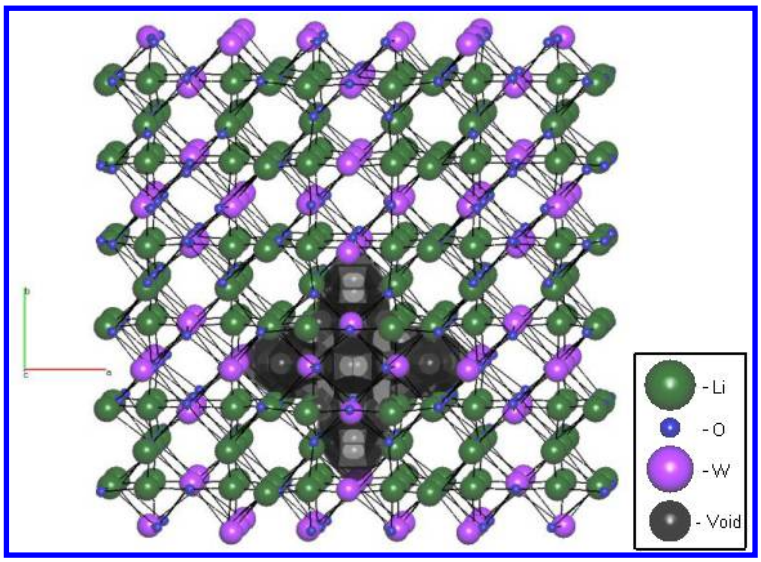

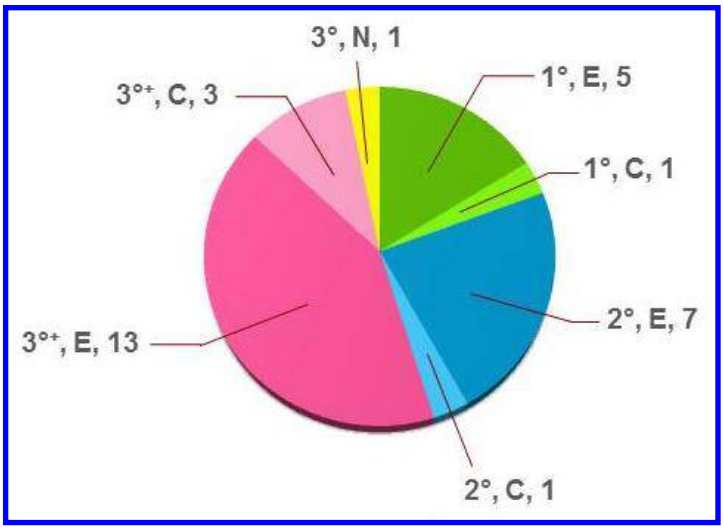

Figure 13. A representative example of a crystal structure (of $Li_2(WO_4)$ [ICSD ref. 10479 – [122]]) displaying the most common (n = 6) n-nodal net in which cages with suitable void space volumes (black/grey) reside to contain Cs^+ ions.

Sr^{2+} ions. The occupancy volume for Sr^{2+} ions (33.51 $Å^3$), was obtained from the Slater empirical radius[44] in TOPOS. Void-space volume requirements for Sr^{2+} ions generated a targeted void space volume of 34 – 38 $Å^3$. Within this range, the suitable cages of 20 previously reported structures bearing 24 cages (5 x 1°; 7 x 2°; 13 x $3°^+$; 3 x multiple cages), five predicted (1 x 1°; 1 x 2°; 3 x $3°^+$), and one new crystal structure, ((**2**), bearing a 3° cage) were identified (Figure 14). A representative example structure that bears a 3-nodal net, the most common type of host framework whose cages appear suited to accommodate Sr^{2+} ions, is shown in Figure 15.

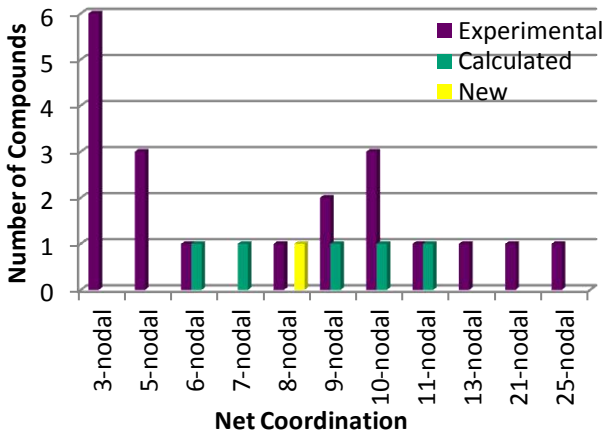

Compound	Cage attribute	Ref. [ICSD - paper]
$CuGd(W_2O_8)$	E, 1°	75006 - [110]
$LiY(W_2O_8)$	E, 1°	156989 - [108]
$Na_5La(WO_4)_4$	E, 1°	20427 - [63]
$Tl_2(WO_4)$	E, 1°	8212 - [80]
$(Bi_2O_2)(W_2O_7)$	E, 1°	88428 - [124]
$CuEr(WO_4)_2$	E, 2°	73747 - [78]
$Rb(NbW_2O_9)$	E, 2°	246143 - [114]
$CuDy_5(WO_4)_8$	E, 2°	380067 - [112]
$Rb_2(WO_4)$	E, 2°	183200 - [113]
$Sc_2(WO_4)_3$	E, 2°	28467 - [118]
$In_2(WO_4)_3$	E, 2°	99606 - [119]
$CuDy(WO_4)_2$	E, 2°- 3°	73749 - [78]
$Cu_2(WO_4)$	E, 3°	202669 - [82]
$Li_2(WO_4)$	E, 3°	160721 - [116]
$Y_2(WO_4)_3$	E, 3°	90938 - [86]
$Ag_{26}I_{18}(WO_4)_4$	E, 3°	56852 - [87]
$Al_2(WO_4)_3$	E, 3°- 4°	73879 - [85]
$(Na_2WO_4)(H_2O)_2$	E, 5°	240882 - [93]
$In_2(WO_4)_3$	E, 6° - 8°	99607 - [119]
$Zr(WO_4)_2$	E, 7°	56566 - [125]
$NaAlW_3O_{11}$	N, 3°	This work – [(**2**)]
$Na_2W_2O_7$	C, 1°	
$Na_2W_2O_7$	C, 2°	
$Na_2W_2O_7$	C, 3°	
$NaAlW_2O_8$	C, 4°	
$Na_2W_2O_7$	C, 6°	

Figure 14. (left) Distribution of cage types (1°, 2°, 3°, $3^{\circ+}$) of host structures comprising n-nodal nets that can incorporate Sr^{2+} ions, according to their frequency observed in previously reported (E) or newly-determined (N) experimental and calculated (C) crystal structures; (right) a list of their associated compound identifiers (ICSD number and reference citation).

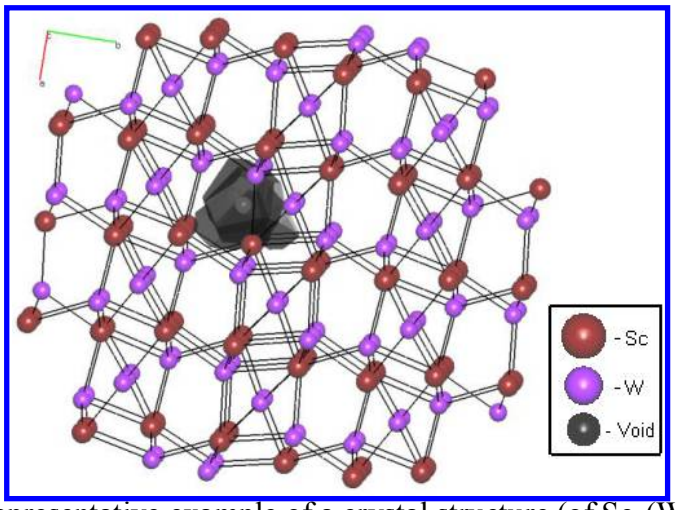

Figure 15. A representative example of a crystal structure (of $Sc_2(WO_4)_3$ [ICSD ref. 28467 – [118]]) manifesting the most common (n = 3) n-nodal net that contains cages with suitable void space volumes (black/grey) to accommodate Sr^{2+} ions.

Alternative Energy Storage.

CH_4 molecules. A target void-space volume of 29 – 33 $Å^3$ for methane was obtained from a kinetic diameter of 3.8 Å.[49] This resulted in the selection of 41 cages from 33 previously reported structures (14 x 1°; 7 x 2°; 20 x 3+°; 7 x multiple cages); 9 cages from 8 predicted structures (2 x 1°; 2 x 2°; 5 x 3+°; 1 x multiple cages), and a 1° cage in the newly-determined structure of (**3**). Figure 16 summarizes these trends. A representative example structure, bearing the most common type of n-nodal net (n = 3) whose cages appear to be able to host CH_4 molecules, is shown in Figure 17.

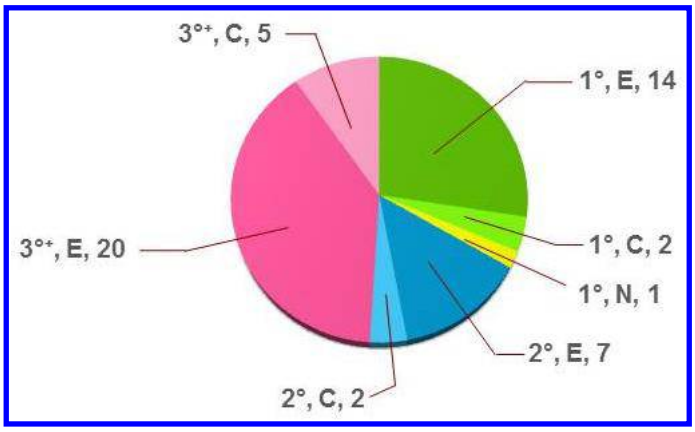

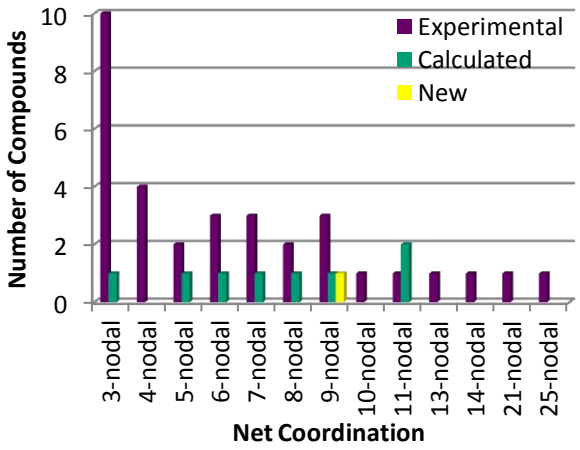

Compound	Cage attribute	Ref. [ICSD - paper]
$CsLiWO_4$	E, 1°	14082 - [126]
$RbGd(WO_4)_2$	E, 1°	152962 - [127]
$KBi(WO_4)_2$	E, 1°	391361 - [128]
$RbNd(WO_4)_2$	E, 1°	155378 - [129]
$K_2(UO_2)(W_2O_8)$	E, 1°	96443 - [130]
$Na_5Tb(WO_4)_4$	E, 1°	20426 - [63]
$Hg(WO_4)$	E, 1°	169667 - [65]
$Li_2(UO_2)_4(WO_4)_4O$	E, 1°	99481 - [131]
$Li_2(WO_4)$	E, 1°	14196 - [132]
Y_2WO_6	E, 1°	261479 - [133]
$K_2(W(O_2)_4)$	E, 1°	202672 - [134]
$Na_2(W_2O_7)$	E, 1°	1883 - [32]
$K_2W_4O_{13}$	E, 1°	2412 - [67]
$Ca_8(Al_{12}O_{24})(WO_4)_2$	E, 1°	62988 - [135]
$U(WO_4)$	E, 2°	2285 - [115]
Cu_2WO_4	E, 2°	62058 - [76]
$Bi_2(WO_6)$	E, 2°	67647 - [136]
$Al_2(WO_4)_3$	E, 2°	73878 - [85]
$La_2(WO_4)_3$	E, 2°	78180 - [137]
$Al_2(WO_4)_3$	E, 2°	90936 - [86]
$(Bi_2O_2)(W_2O_7)$	E, 2° - 3°	88428 - [124]
$CuEr(WO_4)_2$	E, 3°	73747 - [78]
$Rb_4H_8(H_2W_{12}O_{40})(H_2O)_{18}$	E, 3°	16468 - [138]
$Li_2(WO_4)$	E, 3°	15395 - [117]
$Al_2(WO_4)_3$	E, 3°	56827 - [85]
$Sc_2(WO_4)_3$	E, 3° - 4°	28467 - [118]
$In_2(WO_4)_3$	E, 3° - 4°	99606 - [119]
$Cu_2(WO_4)$	E, 4°	202669 - [82]
$Y_2(WO_4)_3$	E, 4° - 5°	90938 - [86]
$Ag_{26}I_{18}(WO_4)_4$	E, 5°	56852 - [87]
$Al_2(WO_4)_3$	E, 5° - 7°	73879 - [85]
$(Na_2WO_4)(H_2O)_2$	E, 6° - 7°	240882 - [93]
$Zr(WO_4)_2$	E, 8° - 9°	56566 - [125]
$Na_2W_2O_7$	N, 1°	This work – [(**3**)]
Na_2WO_4	C, 1°	
$Na_2W_2O_7$	C, 1°	
$NaAlW_2O_8$	C, 2°	
$NaAlW_2O_8$	C, 2°	
$Na_2W_2O_7$	C, 4°	
$Na_2W_2O_7$	C, 5°	
$NaAlW_2O_8$	C, 5° - 6°	
$Na_2W_2O_7$	C, 7°	

Figure 16. (left) Distribution of cage types (1°, 2°, 3+°) of host structures comprising n-nodal nets that can incorporate CH_4 molecules, according to their frequency observed in previously reported (E) or newly-determined (N) experimental and calculated (C) crystal structures; (right) a list of their associated compound identifiers (ICSD number and reference citation).

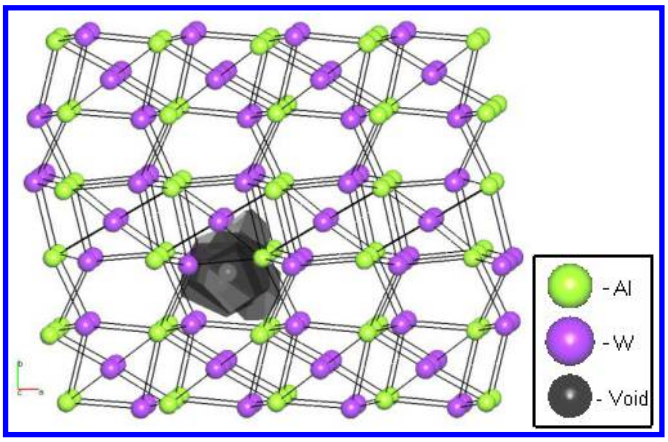

Figure 17. A representative example of a crystal structure (of $Al_2(WO_4)_3$ [ICSD ref. 90936 – [86]]) illustrating the most common n-nodal (n = 3) net in which cages with suitable void space volumes (black/grey) can host CH_4 molecules.

H_2 molecules. The target volume of H_2 was determined using a kinetic diameter of 2.89 Å,[19] resulting in a target void-space volume range of 13 – 17 $Å^3$. 190 suitable cages to host H_2 were found in 124 previously reported structures (48 x 1°; 39 x 2°; 103 x $3°^+$; 39 x multiple cages); 39 cages in 23 predicted structures (4 x 1°; 5 x 2°; 30 x $3°^+$; 11 x multiple cages); and the in-house determined crystal structure, (**3**) (4°); as seen in Figure 18. Interestingly, eight of the previously reported, as well as one of the predicted structures, each contain at least four suitable types of cages for hosting H_2. Figure 19 displays a representative example of a tungstate-based framework structure bearing the most common n-nodal set (n = 3) with suitable cages to host H_2 molecules.

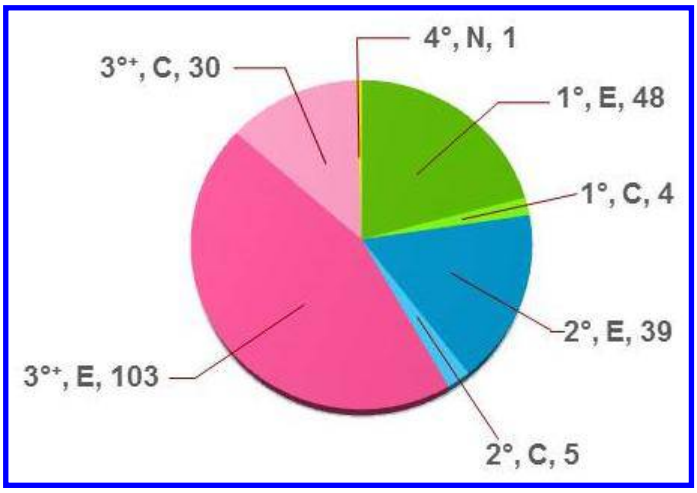
4°, N, 1
3°+, C, 30
1°, E, 48
1°, C, 4
2°, E, 39
3°+, E, 103
2°, C, 5

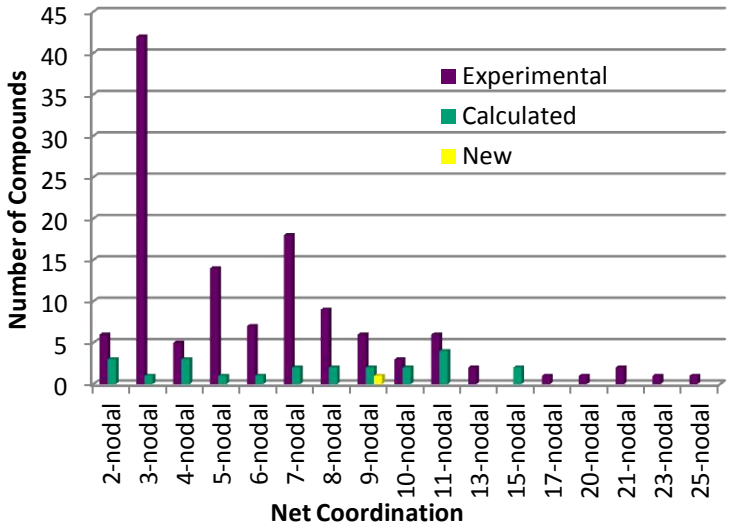
Number of Compounds
45
40
35
30
25
20
15
10
5
0
Experimental
Calculated
New
2-nodal
3-nodal
4-nodal
5-nodal
6-nodal
7-nodal
8-nodal
9-nodal
10-nodal
11-nodal
13-nodal
15-nodal
17-nodal
20-nodal
21-nodal
23-nodal
25-nodal
Net Coordination

Compound	Cage attribute	Ref. [ICSD -paper]
$Li(NbWO_6)$	E, 1°	202779 - [139]
$Li(NbWO_6)$	E, 1°	202780 - [139]
$K((SbW)O_6)$	E, 1°	181570- [140]
$Cs(SbWO_6)$	E, 1°	165063 - [141]
$KNb(WO_6)$	E, 1°	63562- [142]
$AgIn(WO_4)_2$	E, 1°	60373- [143]
$LiLaW_2O_8$	E, 1°	261829- [144]
$LiGdW_2O_8$	E, 1°	261833- [144]
$LiSmW_2O_8$	E, 1°	261831 - [144]
$LiEuW_2O_8$	E, 1°	261832 - [144]
$LiNdW_2O_8$	E, 1°	261830 - [144]
$Cs(TaWO_6)$	E, 1°	165061- [141]
$NaBi(WO_4)_2$	E, 1°	168136- [145]
$Pb_2Co(WO_6)$	E, 1°	77912 - [146]
$Sr_2Zn(WO_6)$	E, 1°	72811 - [147]
$Sr_2Mg(WO_6)$	E, 1°	152575 - [148]
$Ba_2(CoWO_6)$	E, 1°	97029 - [149]
Ba_2CoWO_6	E, 1°	27425 - [150]
Ba_2NiWO_6	E, 1°	27426 - [150]
$Ba_2(FeWO_6)$	E, 1°	95520 - [151]
$Pb_2Mg(WO_6)$	E, 1°	67880 - [152]
Ba_2ZnWO_6	E, 1°	423034 - [153]
$Ba_2Ca(WO_6)$	E, 1°	245599 - [154]
$NaIn(WO_4)_2$	E, 1°	16263 - [155]
$Ni(WO_4)$	E, 1°	16685 - [156]
$CrWO_4$	E, 1°	36213 - [157]
$Ca(WO_4)$	E, 1°	155424 - [158]
$Ca(WO_4)$	E, 1°	155423 - [158]
$NaIn(WO_4)_2$	E, 1°	28098 - [159]
$Sr(WO_4)$	E, 1°	155425 - [158]
$Pb(WO_4)$	E, 1°	155522 - [160]
$Ba(WO_4)$	E, 1°	155513 - [160]
$Pb_2Co(WO_6)$	E, 1°	72905 - [161]
Ba_2MgWO_6	E, 1°	423033 - [153]
$Na_2(WO_4)$	E, 1°	44524 - [162]
$Hg(WO_4)$	E, 1°	169671 - [65]
$Nd(WO_3N)$	E, 1° - 2°	99740 - [163]
$NaDy(WO_4)_2$	E, 1° - 2°	248012 - [164]
$NaBi(WO_4)_2$	E, 1° - 2°	83318 - [165]
$NaNd(WO_4)_2$	E, 1° - 2°	66091 - [166]
$NaGd(WO_4)_2$	E, 1° - 2°	157390 - [167]
$NaLa(WO_4)_2$	E, 1° - 2°	66090 - [166]
$Pb(WO_4)$	E, 1° - 2°	75981 - [168]
$(LiLa)(WO_4)_2$	E, 1° - 2°	184015 - [169]
$Sr(WO_4)$	E, 1° - 3°	155426 - [158]
$Pb(WO_4)$	E, 1° - 3°	155518 - [160]
$Na_2ZrW_3O_{12}$	E, 1° - 3°	20405 - [170]
$Eu_3(BWO_9)$	E, 1° - 4°	39810 - [171]
$KLa(WO_4)_2$	E, 2°	95541 - [172]
$CsLu(WO_4)_2$	E, 2°	202270 - [173]
$KEu(WO_4)_2$	E, 2°	173634 - [53]
$KLu(WO_4)_2$	E, 2°	172510 - [95]
$KYb(WO_4)_2$	E, 2°	280877 - [96]
$KEr(WO_4)_2$	E, 2°	157832 - [97]
$KY(WO_4)_2$	E, 2°	411285 - [98]
$KHo(WO_4)_2$	E, 2°	182626 - [99]
$Ba(TeW_2O_9)$	E, 2°	281502 - [174]
$La_3(BWO_9)$	E, 2°	39809 - [171]
$Eu_3(BWO_9)$	E, 2°	150338 - [175]
$Dy_3(BWO_9)$	E, 2°	250419 - [55]
$Tb_3(BWO_9)$	E, 2°	250418 - [55]
$Gd_3(BWO_9)$	E, 2°	250417 - [55]
$Nd_3(BWO_9)$	E, 2°	250415 - [55]
$Sm_3(BWO_9)$	E, 2°	250416 - [55]
$Pr_3(BWO_9)$	E, 2°	250414 - [55]
$KBi(WO_4)_2$	E, 2°	391361 - [128]
$La_2(WO_4)(Te_3O_7)_2$	E, 2°	249538 - [58]
$Ba_{11}(W_4O_{23})$	E, 2°	418207 - [56]
Y_2WO_6	E, 2°	261479 - [133]
$K_2(TeW_3O_{12})$	E, 2°	97506 - [176]
$Rb_2(W_2O_7)$	E, 2°	300230 - [177]
$Hg(WO_4)$	E, 2°	169667 - [65]
LiW_3O_9	E, 2° - 3°	38310 - [178]
$Li_2(UO_2)(WO_4)_2$	E, 2° - 3°	99480 - [131]

Compound	Cage attribute	Ref. [ICSD - paper]
$NdNa_5(WO_4)_4$	E, 2°- 4°	6145 - [179]
$BiLaWO_6$	E, 3°	416793 - [52]
$BiNdWO_6$	E, 3°	416789 - [52]
$Pr_3(WO_6)Cl_3$	E, 3°	20626 - [105]
$La_3WO_6Cl_3$	E, 3°	35595 - [106]
$LiY(W_2O_8)$	E, 3°	156989 - [108]
$KNd(WO_4)_2$	E, 3°	9364 - [180]
$Ca_3WO_5Cl_2$	E, 3°	2335 - [181]
$Li_2(UO_2)_4(WO_4)_4O$	E, 3°	99481 - [131]
$Nd(WO_4)(OH)$	E, 3°	27731 - [182]
$Pb_6B_2WO_{12}$	E, 3°	261534 - [183]
$Rb_2(TeW_3O_{12})$	E, 3°	97507 - [176]
$K_2(UO_2)(W_2O_8)$	E, 3° - 5°	96443 - [130]
$Li_2Cu(WO_4)_2$	E, 3° - 5°	92854 - [101]
$Na_4Th(WO_4)_4$	E, 3° - 5°	422185 - [61]
$Li_2Ni(WO_4)_2$	E, 3° - 5°	92853 - [101]
$Li_2Co(WO_4)_2$	E, 3° - 6°	92852 - [101]
$Na_2W_2O_7(H_2O)$	E, 3° - 6°	408189 - [184]
$Na_3F(WO_4)$	E, 4°	417289 - [73]
$Rb_4H_8(H_2W_{12}O_{40})(H_2O)_{18}$	E, 4°	16468 - [138]
$Na_2(W_2O_7)$	E, 4°	1883 - [32]
$K_2W_4O_{13}$	E, 4°	2412 - [67]
$Ca_8(Al_{12}O_{24})(WO_4)_2$	E, 4°	71806 - [123]
UW_3O_{11}	E, 4°	81983 - [75]
$ErBi(W_2O_9)$	E, 4° - 5°	183443 - [72]
$EuBi(W_2O_9)$	E, 4° - 5°	183444 - [72]
$Rb_2(WO_4)$	E, 4° - 5°	183200 - [113]
$Li_2(W_2O_7)$	E, 4° - 5°	1897 - [71]
$SmBi(W_2O_9)$	E, 4° - 5°	183445 - [72]
Bi_2WO_6	E, 4° - 6°	171328 - [102]
$Na_5Lu(WO_4)_4$	E, 4° - 7°	200930 - [62]
$Na_5Tb(WO_4)_4$	E, 4° - 7°	20426 - [63]
$Rb_{12}(Nb_{30}W_3O_{90})$	E, 5°	1505 - [107]
$CuGd(W_2O_8)$	E, 5° - 6°	75006 - [110]
$LiPr(WO_4)_2$	E, 5° - 6°	200520 - [111]
$Na_5Y(WO_4)_4$	E, 5° - 9°	417143 - [74]
$Na_5La(WO_4)_4$	E, 5° - 9°	20427 - [63]
$CuDy(WO_4)_2$	E, 6°	73749 - [78]
$CuEr(WO_4)_2$	E, 6°	73747 - [78]
$CuSm(W_2O_8)$	E, 6°	68615 - [79]
$CuLa(W_2O_8)$	E, 6° - 7°	68614 - [79]
$Al_2(WO_4)_3$	E, 7°	73878 - [85]
$Al_2(WO_4)_3$	E, 7°	90936 - [86]
$Sc_2(WO_4)_3$	E, 7°	28467 - [118]
$U(WO_4)$	E, 7° - 8°	2285 - [115]
$K_2Nb_{10}W_7O_{47}$	E, 7° - 8°	62130 - [84]
$Cu_2(WO_4)$	E, 7° - 10°	202669 - [82]
$Ce_{10}W_{22}O_{81}$	E, 8° - 10°	260095 - [81]
$Ag_{26}I_{18}(WO_4)_4$	E, 9°	56852 - [87]
$FeCe(WO_4)(W_2O_8)$	E, 9° - 10°	401919 - [83]
$Na_2W_2O_7$	N, 4°	This work – [(**3**)]
$NaAlW_2O_8$	C, 1°	
$NaAlW_2O_8$	C, 1° - 2°	
$NaAlW_2O_8$	C, 1° - 2°	
$NaAlW_2O_8$	C, 1° - 2°	
Na_2WO_4	C, 2°	
$Na_2W_2O_7$	C, 2° - 3°	
Na_2WO_4	C, 3°	
Na_2WO_4	C, 3°	
$Na_2W_2O_7$	C, 3°	
Na_4WO_5	C, 3° - 4°	
$Na_2W_2O_7$	C, 4°	
$Na_2W_4O_{13}$	C, 4°	
$NaAlW_2O_8$	C, 4°	
$Na_2W_2O_7$	C, 5°	
Na_2WO_4	C, 5° - 6°	
$NaAlW_2O_8$	C, 5° - 6°	
$NaAlW_2O_8$	C, 5° - 7°	
$Na_2W_2O_7$	C, 5° - 9°	
$Na_2W_4O_{13}$	C, 6°	
$NaAlW_2O_8$	C, 6°	
$NaAlWO_5$	C, 6° - 7°	

$NaAlW_2O_8$	C, 6° - 8°
$Na_2W_2O_7$	C, 10°

Figure 18. (top) Distribution of cage types (1°, 2°, $3^{\circ+}$, 4°) of host structures comprising n-nodal nets that can incorporate H_2 molecules, according to their frequency observed in previously reported (E) or newly-determined (N) experimental and calculated (C) crystal structures; (bottom) a list of their associated compound identifiers (ICSD number and reference citation).

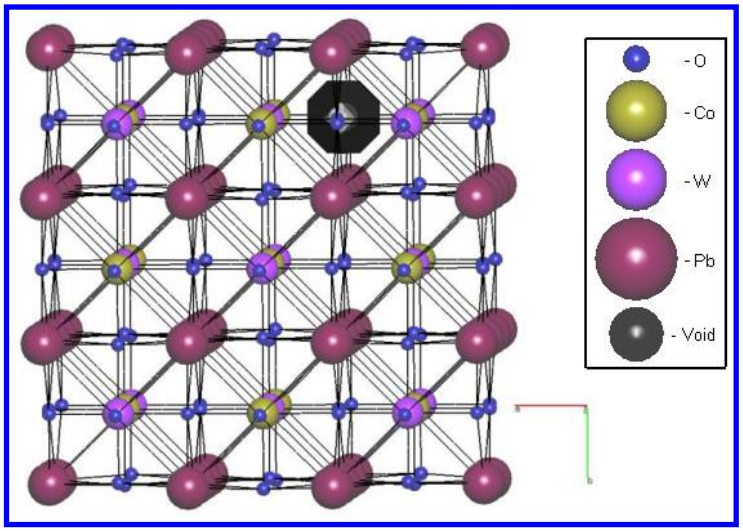

Figure 19. A representative example of a crystal structure (of $Pb_2Co(WO_6)$ [ICSD ref. 72905 – [161]]) displaying the most common n-nodal (n = 3) net in which cages with suitable void space volumes (black/grey) can host H_2 molecules.

General trends

Topological patterns and frequency trends in guest-host matching preferences. One of the main objectives of this study was the discovery of potential trends in topological patterns of tungstate framework structures with respect to their desired guest type. The results of the

experimentally-determined structures clearly demonstrate that for smaller (H_2, U or Pu) and medium-sized (CH_4, or Sr^{2+}) guests, compounds with 3-nodal nets are the most abundant. In this context, the small guest molecule CO_2 is an exception since it prefers 5- and 6-nodal structures. Within each of the predominant net classifications, the majority of the best suited cages for guests were found to be 3°, aside from those involving the two smallest guest types. Here, CO_2 is best hosted almost exclusively in 1°, 2°, or 3° cages of 5- or 6-nodal nets, whereas H_2 finds suitable host accommodation predominantly in the 1° cages of 3-nodal nets. It transpires that the three largest guests, PuO_2, UO_2, and Cs^+, prefer higher-nodal nets, and they can be hosted exclusively in 1° cages within their preferred n-nodal nets.

In contrast, computationally-derived structures indicate that tungstate frameworks with higher-order nodal nets are preferred hosts, and several guest types (CO_2, H_2, CH_4) showed promise for their inclusion into 11-nodal net structures. The preferred hosts for U and Pu ions were 4-nodal nets, whereas Cs^+ preferred 6-nodal nets. For PuO_2, and UO_2 only one calculated structure, featuring an 8-nodal, and a 10-nodal net, respectively, was deemed a suitable host, while Sr^{2+} guests did not exhibit any dominant net-type for their host structures.

Experimentally-derived versus hypothetical tungstates structures: trends and biases. This discrepancy in host-guest matching preferences between predicted- and experimentally-determined structures may arise from a variety of factors. Firstly, this is a rather complicated comparison, given that the computationally-determined hypothetical structures exclusively considered possible variations of $Na_aAl_bW_cO_d$ (where a, c, d may be any integer and b may be any integer or zero), whereas the generated set of experimentally-determined structures was far less restrictive: including any structure that contains W, O, and one or two other elements. The host-guest matching preferences determined using the computationally-derived structural set might naturally be refined if hypothetical tungstate structures were

generated for all of the possible chemical compositions that are accepted in the experimentally-derived structural set; although such a quest would be computationally expensive and laborious. So turning this problem on its head, if all compounds with the general formula $Na_aX_bW_cO_d$ (where X is any element) are isolated from the experimentally-derived structural data set, a preference trend towards nets of higher order - mostly 5-, 8-, and 9-nodal nets - can be observed, *i.e.* experimental and computational results apparently tend towards a common preference of higher-order nodal nets as suitable hosts. However, with one exception, these trends have to be considered with caution, owing to the very limited numbers of compounds available for each guest type as a result of this data restriction. The exception concerns the set of possible hosts for H_2; in this case, 3-nodal nets remained preferred for both the full experimental findings and within this experimental source restriction to $Na_aX_bW_cO_d$.

Secondly, this host-guest matching preference discrepancy may be due to the generated cage volumes in the theoretically-calculated structures, which were typically larger than those encountered in experimentally determined structures. Nonetheless, observed differences are cage size and type dependent. For example, primary cages for the largest cage sizes compare well between hypothetically and experimentally generated structures (329.35 $Å^3$ and 326.95 $Å^3$, respectively, on average). Discord appears more at the detailed level and this reflects more of a classification problem than a straight-forward difference between theory and experiment. This can be illustrated by a consideration of some primary cage statistics. If these primary cage sizes are separated into volumes ranges, and a percentage is constructed for the number of primary cages found in each volume range versus the total number of primary cages, differences become more apparent. In this respect, experimental structures have 8% of primary cages in the >100 $Å^3$ range, 16% within 50-100 $Å^3$, 31% within 20-50 $Å^3$, and 45%

<20 Å^3. In contrast, calculated structures have 35% of primary cages in the >100 Å^3 range, 23% within 50-100 Å^3, 33% within 20-50 Å^3, and 9% <20 Å^3. In addition, a greater number of distinct cages were found in many cases for the theoretically calculated structures. Again, some statistics are helpful for explanation: 62.3% of experimental structures possess 1-10 total cages, 24.3% have 11-20 total cages, 8.1% have 21-30 total cages, 4.2% have 31-40 total cages, 0.7% have 41-50 total cages, and 0.4% have >50 total cages. In contrast, 18.6% of calculated structures have 1-10 total cages, 39.5% have 11-20 total cages, 14.0% have 21-30 total cages, 9.3% have 31-40 total cages, 2.3% have 41-50 total cages, and 16.3% have >50 total cages. Furthermore, despite comprising a higher absolute number of cages, often fewer cages of distinct volumes were found for the calculated relative to the experimental structures owing to many cages numerically producing the same volume as other cages within a single structure.

Thirdly, databases of experimentally-determined crystal structures contain an intrinsic chemical bias since the determination of a crystal structure is predicated on a systematic distortion of chemical space, on several accounts. For example, some classes of chemicals are easier to crystallize than others, and obtaining crystals of a compound naturally facilitates its likelihood of associated crystal structure determination. Certain families of compounds will also appear in a crystal structure database with greater frequency than others, or even exist in duplicate or manifold. Possible causes of this include synthetic efforts being prolific in a specific area of chemistry where compounds are in vogue for a popular application; or the prevalence of polymorphism in a series of chemicals that issues duplicate chemical structures that bear different space groups.

In the context of the subject study, this chemical bias could manifest as clusters of preferred nets owing to the large grouping of chemical families with similar structures. Indeed, such

clustering is borne out in this study. One example of it features in the list of 'ideal net' compounds that could host H_2, which includes five compounds with the formula $LiXW_2O_8$ (X = lanthanide). These families of compounds will naturally form similar nets, as their chemical connectivity is similar. Another example concerns the possible hosts for CH_4, amongst which four different space groups of $Al_2(WO_4)_3$ can be found: Pbcn, Pnca, $P2_1/n$, and $P2_1$, i.e. the replication of chemical formula but distinguished by polymorphism. Again, all of these result in the same, or similar, nets.

While computationally-derived structural data sets also have the ability to feature chemical bias, such bias would have to be generated by the user, and good practice in computational research is usually able to circumvent any significant biases at the level of those present in large sets of experimental data. This experimental bias therefore augments the level of discrepancy between experimental and computationally derived host-guest matching preferences.

How do the in-house determined crystal structures (1)-(3) rate as potential hosts and present within the broader set of tungstate structural frameworks? The in-house determined crystal structure of (**1**) contained only two cages: one relatively large (66.03 $Å^3$), and a relatively small one (5.28 $Å^3$). These cages were only able to accommodate one of the guest types (UO_2) explored in this study. The crystal structure of (**1**) represents the first report of its structural type for the formula, $NaAlW_2O_8$. Hypothetical structures that conformed to the same formula, but exhibited different frameworks, were nonetheless identified; and when taken collectively, they were predicted to be able to accommodate all but two guest types (PuO_2, and UO_2).

Void-space analysis indicates that the crystal structure of (**2**) can accommodate PuO_2, UO_2, or Sr^{2+}. The rarity of this crystal structure is even more stark than that of (**1**), being the first report of any structural type with formula, $NaAlW_3O_{11}$. The fact that not even any hypothetical structures of this formula were predicted via the computational aspect of this study is particularly interesting. As noted earlier, the fundamental strategy behind the structure prediction method used herein is based on the statistical likelihood of ionic substitution of previously reported crystal structures. The lack of any hypothetical structures of this formula in its prediction set is therefore symptomatic of no other previously reported experimental structures of this formula well beyond just tungstates. It would thus seem that the crystal structure of (**2**) is rare indeed, to the extent that it could now be used as an exemplar to help ionic substitution methods start to predict isomorphous structures of other (non-tungstate) inorganic frameworks. The structure determination of (**2**) was in fact particularly challenging, and so the use of this first structural exemplar in concert with this type of structural prediction method could go one step further, by offering computation the possibility to help guide the experimental crystallographer to probable solutions of isomorphous structures. An example of such a concerted approach, whose premise is built upon similar lines, is that of Meredig and Wolverton.[185]

Among the three in-house determined crystal structures, (**3**) offers the most options for hosting the guests explored in this study, being able to accommodate U or Pu ions as well as CH_4 and H_2 molecules. In addition, the corresponding hypothetical structures of $Na_2W_2O_7$ were able to host all guests, except for PuO_2, in at least one manifestation of this chemical formula. It is worth remembering that the room-temperature crystal structure of (**3**) has been reported previously, so statistical inferences behind the structure prediction method used in this study are facilitated with pre-existing crystal structure evidence. The fact that (**3**) differs

from (**1**) and (**2**) by its chemical lack of Al is presumably also significant to the nature of these host-guest matching preferences. In any event, the finding that (**3**) offers the most abundant selection of host-guest matching preferences amongst our three in-house available materials, means that we now have a practical guide forward for prioritizing experimental host-guest adsorption studies on these compounds.

Concluding remarks and future outlook

Void space analysis of 577 tungstate crystal structures, mined from experimentally- and computationally-derived data sources, offers an important first step towards identifying new host materials for environmentally important small molecules and ions. 196 hypothetical tungstate structures were generated using the recently developed structure prediction methods that exploit the statistical likelihood of ionic substitution;[38] 378 experimentally determined crystal structures of tungstates were sourced from the ICSD and coupled with three in-house crystal structure determinations of tungstate materials, (**1**)-(**3**). It transpired that $NaAlW_2O_8$ (**1**) and $NaAlW_3O_{11}$ (**2**) present somewhat rare crystal structures; and while (**2**) appears well suited to host several nuclear waste materials, $Na_2W_2O_7$ (**3**) is predisposed to accommodate small molecules, CH_4 and H_2, for alternative energy applications, as well as industrially relevant ions for containing nuclear waste.

Beyond the immediate practical considerations of these three in-house available materials, the data-mining aspect of this study pinpoints a number of other tungstate framework structures that can, when taken collectively, host the entire range of environmentally important molecules and ions explored in this study (CO_2, UO_2, PuO_2, U, Pu, Cs^+, Sr^{2+}, CH_4, and H_2). To this end, these results offer good prospects for tungstate compounds as viable host materials for environmental storage applications. Some of these other tungstate structures

may even host certain guests better than the in-house tungstate materials immediately available to us. However, the scope of this study essentially provides a binary outcome for a given framework structure: either the structure is, or is not, able to host a given guest. While this study illustrates a preference to certain types of n-nodal structures by virtue of their observed frequency, this does not imply directly that these preferred hosts are superior to those less commonly found. There are currently no formal ranking criteria that define one tungstate compound over another as being better able to host a given type of guest. It would be natural to develop such a ranking formalism as these void-space analysis methods continue to evolve. To this end, comparison with other host/guest prediction methods, such as channel evaluation,[26] or substructural similarity functions[186] might prove useful. This will further assist the experimentally-minded materials scientist in selecting their host material to most optimally store small, but environmentally important, molecules or ions.

Notwithstanding the powerful practical bearing of generating a catalogue of material selections that could ultimately allow one to simply 'dial up' a request to match a host structure to a desired guest, it should also be remembered that the currently predicted host frameworks have hypothetical as well as experimental crystal structure origins, so some of these tungstate materials have yet to be experimentally realized; the combined sets of experimentally and computationally generated data are also currently limited. In the spirit of considering further developments of this approach, a more explicit parameterization of guest shape may also help to refine the host-guest matching preferences predicted by this study.

Looking ahead, it should be remembered that this study has only shown how to physically fit guest types into cages of host structures; it has not considered the fabrication method of the host-guest composite. Indeed, this is a study in its own right, and much research has been engaged with studying the dynamic processes associated with adsorption of a specific guest

into an individual host;[187,188] or nanofabrication routes that render *in situ* host-guest synthesis where the guest is embedded into the host in a concerted fashion.[189,190] The subject study represents more of a 'ship in a bottle' perspective, considering the final outcome, pending the experimental adsorption conditions (heat, pressure, reaction phase, etc) or concerted host-guest nanofabrication methods can be resolved. Ideally, this 'ship in a bottle' approach, which surveys a broad set of structures, will ultimately go hand-in-hand with simulations of adsorption dynamics or nanofabrication of individual guest-host composites, that can be short-listed via our procedure; with auxiliary considerations that ensure chemical compatibility between host and guest. Creating such a unified effort will enable an 'all-in-one' prediction of molecular storage capabilities and its associated synthetic processing.

Acknowledgements

Velin Nikolov from the Bulgarian Academy of Sciences is gratefully acknowledged for supplying the samples of tungstate materials (**1**)-(**3**). John J. Rickard from the Cavendish Laboratory, University of Cambridge, is thanked for his technical assistance with the EDX experiment. J. M. C. is indebted to the Fulbright Commission for a UK-US Fulbright Scholar Award hosted by Argonne National Laboratory where work done was supported by DOE Office of Science, Office of Basic Energy Sciences, under Contract No. DE-AC02-06CH11357.

Supplementary Information Crystallographic information files for (**1**)-(**3**) are provided as Supplementary Information and are available from the corresponding author.

References

(1) Pires, J.; Carvalho, A.; de Carvalho, M. B. Adsorption of Volatile Organic Compounds in Y Zeolites and Pillared Clays. *Microporous Mesoporous Mater.* **2001**, *43* (3), 277–287._

(2) Shu, H.-T.; Li, D.; Scala, A. A.; Ma, Y. H. Adsorption of Small Organic Pollutants from Aqueous Streams by Aluminosilicate-Based Microporous Materials. *Sep. Purif. Technol.* **1997**, *11* (1), 27–36.

(3) Millward, A. R.; Yaghi, O. M. Metal-Organic Frameworks with Exceptionally High Capacity for Storage of Carbon Dioxide at Room Temperature. *J. Am. Chem. Soc.* **2005**, *127* (51), 17998–17999.

(4) Drabarek, E.; McLeod, T. I.; Hanna, J. V.; Griffith, C. S.; Luca, V. Tungstate-Based Glass–ceramics for the Immobilization of Radio Cesium. *J. Nucl. Mater.* **2009**, *384* (2), 119–129.

(5) Luca, V.; Griffith, C. S.; Drabarek, E.; Chronis, H. Tungsten Bronze-Based Nuclear Waste Form Ceramics. Part 1. Conversion of Microporous Tungstates to Leach Resistant Ceramics. *J. Nucl. Mater.* **2006**, *358* (2-3), 139–150.

(6) Luca, V.; Drabarek, E.; Chronis, H.; McLeod, T. Tungsten Bronze-Based Nuclear Waste Form Ceramics. Part 3: The System Cs0.3MxW1−xO3 for the Immobilization of Radio Cesium. *J. Nucl. Mater.* **2006**, *358* (2-3), 164–175.

(7) Griffith, C. S.; Sebesta, F.; Hanna, J. V.; Yee, P.; Drabarek, E.; Smith, M. E.; Luca, V. Tungsten Bronze-Based Nuclear Waste Form Ceramics. Part 2: Conversion of Granular Microporous Tungstate–polyacrylonitrile (PAN) Composite Adsorbents to Leach Resistant Ceramics. *J. Nucl. Mater.* **2006**, *358* (2-3), 151–163.

(8) Eddaoudi, M.; Kim, J.; Rosi, N.; Vodak, D.; Wachter, J.; O'Keeffe, M.; Yaghi, O. M. Systematic Design of Pore Size and Functionality in Isoreticular MOFs and Their Application in Methane Storage. *Science* **2002**, *295* (5554), 469–472.

(9) Msayib, K. J.; Book, D.; Budd, P. M.; Chaukura, N.; Harris, K. D. M.; Helliwell, M.; Tedds, S.; Walton, A.; Warren, J. E.; Xu, M.; et al. Nitrogen and Hydrogen Adsorption by an Organic Microporous Crystal. *Angew. Chemie* **2009**, *121* (18), 3323–3327.

(10) Furukawa, H.; Yaghi, O. M. Storage of Hydrogen, Methane, and Carbon Dioxide in Highly Porous Covalent Organic Frameworks for Clean Energy Applications. *J. Am. Chem. Soc.* **2009**, *131* (25), 8875–8883.

(11) Chun, H.; Moon, J. Discovery, Synthesis, and Characterization of an Isomeric Coordination Polymer with Pillared Kagome Net Topology. *Inorg. Chem.* **2007**, *46* (11), 4371–4373.

(12) Li, H.; Eddaoudi, M.; O'Keeffe, M.; Yaghi, O. M. Design and Synthesis of an Exceptionally Stable and Highly Porous Metal-Organic Framework. *Nature* **1999**, *402* (6759), 276–279.

(13) Ockwig, N. W.; Delgado-Friedrichs, O.; O'Keeffe, M.; Yaghi, O. M. Reticular Chemistry: Occurrence and Taxonomy of Nets and Grammar for the Design of Frameworks. *Acc. Chem. Res.* **2005**, *38* (3), 176–182.

(14) O'Keeffe, M.; Yaghi, O. M. Deconstructing the Crystal Structures of Metal-Organic Frameworks and Related Materials into Their Underlying Nets. *Chem. Rev.* **2012**, *112* (2), 675–702.

(15) Rosi, N. L.; Eckert, J.; Eddaoudi, M.; Vodak, D. T.; Kim, J.; O'Keeffe, M.; Yaghi, O. M. Hydrogen Storage in Microporous Metal-Organic Frameworks. *Science* **2003**, *300* (5622), 1127–1129.

(16) Tranchemontagne, D. J.; Mendoza-Cortés, J. L.; O'Keeffe, M.; Yaghi, O. M. Secondary Building Units, Nets and Bonding in the Chemistry of Metal-Organic Frameworks. *Chem. Soc. Rev.* **2009**, *38* (5), 1257–1283.

(17) Wong-Foy, A. G.; Matzger, A. J.; Yaghi, O. M. Exceptional H2 Saturation Uptake in Microporous Metal-Organic Frameworks. *J. Am. Chem. Soc.* **2006**, *128* (11), 3494–3495.

(18) Menon, V.; Komarneni, S. Porous Adsorbents for Vehicular Natural Gas Storage: A Review. *J. Porous Mater.* **1998**, *58*, 43–58.

(19) Rowsell, J. L. C.; Yaghi, O. M. Strategies for Hydrogen Storage in Metal--Organic Frameworks. *Angew. Chem. Int. Ed. Engl.* **2005**, *44* (30), 4670–4679.

(20) Wang, B.; Côté, A. P.; Furukawa, H.; O'Keeffe, M.; Yaghi, O. M. Colossal Cages in Zeolitic Imidazolate Frameworks as Selective Carbon Dioxide Reservoirs. *Nature* **2008**, *453* (7192), 207–211.

(21) Luebbers, M. T.; Wu, T.; Shen, L.; Masel, R. I. Trends in the Adsorption of Volatile Organic Compounds in a Large-Pore Metal-Organic Framework, IRMOF-1. *Langmuir* **2010**, *26* (13), 11319–11329.

(22) Yang, K.; Sun, Q.; Xue, F.; Lin, D. Adsorption of Volatile Organic Compounds by Metal-Organic Frameworks MIL-101: Influence of Molecular Size and Shape. *J. Hazard. Mater.* **2011**, *195*, 124–131.

(23) Côté, A. P.; Benin, A. I.; Ockwig, N. W.; O'Keeffe, M.; Matzger, A. J.; Yaghi, O. M. Porous, Crystalline, Covalent Organic Frameworks. *Science* **2005**, *310* (5751), 1166–1170.

(24) Ewing, R. C. The Design and Evaluation of Nuclear-Waste Forms: Clues from Mineralogy. *Can. Mineral.* **2001**, *39* (June), 697–715.

(25) Hamdi, B.; Houari, M.; Hamoudi, S.; Kessaïssia, Z. Adsorption of Some Volatile Organic Compounds on Geomaterials. *Desalination* **2004**, *166*, 449–455.

(26) Anurova, N.; Blatov, V.; Ilyushin, G.; Blatova, O.; Ivanovschitz, a; Demyanets, L. Migration Maps of Li+ Cations in Oxygen-Containing Compounds. *Solid State Ionics* **2008**, *179* (39), 2248–2254.

(27) Blatov, V. A. Nanocluster Analysis of Intermetallic Structures with the Program Package TOPOS. *Struct. Chem.* **2012**, *23* (4), 955–963.

(28) Pöyry Energy Limited. *The 2007 UK Radioactive Waste Inventory: A Review of the Processes Contributing to Radioactive Wastes in the UK*; 2008.

(29) Griffith, C. S.; Luca, V. Ion-Exchange Properties of Microporous Tungstates. *Chem. Mater.* **2004**, *16* (24), 4992–4999.

(30) Forsberg, C. W. Rethinking High-Level Waste Disposal : Separate Disposal of High-Heat Radionuclides (^{90}Sr and ^{137}Cs) Management and Disposal. *Nucl. Technol.* **2008**, *131* (2), 252–268.

(31) Nikolov, I.; Nikolov, V.; Peshev, P. Regions of Phase Crystallization and New Double Tungstates in the System Na2O–Al2O3–WO3. *J. Alloys Compd.* **2003**, *351* (1-2), 202–207.

(32) Okada, K.; Morikawa, H.; Marumo, F.; Iwai, S. Disodium Ditungstate. *Acta Crystallogr. Sect. B Struct. Crystallogr. Cryst. Chem.* **1975**, *31* (4), 1200–1201.

(33) Otwinowski, Z.; Minor, W. Processing of X-ray Diffraction Data Collected in Oscillation Mode. In *Methods in Enzymology, Volume 276: Macromolecular Crystallography, Part A*, pp307-326; Carter, C. W. Jr., Sweet R. M., Eds.; Academic Press: New York, **1997**.

(34) Blessing, R. H. An Empirical Correction for Absorption Anisotropy. *Acta Crystallogr. A.* **1995**, *51 (Pt 1)* (1), 33–38.

(35) Rigaku Americas and Rigaku. CrystalClear-SM Expert 2.0 software, **2009**.

(36) Higashi, T. ABSCOR, Rigaku Corporation, Tokyo, Japan, **1995**.

(37) Sheldrick, G. M. A Short History of SHELX. *Acta Crystallogr. A.* **2008**, *64* (Pt 1), 112–122.

(38) Hautier, G.; Fischer, C.; Ehrlacher, V.; Jain, A.; Ceder, G. Data Mined Ionic Substitutions for the Discovery of New Compounds. *Inorg. Chem.* **2011**, *50*, 656–663.

(39) Delgado-Friedrichs, O.; O'Keeffe, M. Crystal Nets as Graphs: Terminology and Definitions. *J. Solid State Chem.* **2005**, *178* (8), 2480–2485.

(40) Bonneau, C.; Delgado-Friedrichs, O.; O'Keeffe, M.; Yaghi, O. M. Three-Periodic Nets and Tilings: Minimal Nets. *Acta Crystallogr. A.* **2004**, *60* (Pt 6), 517–520.

(41) Blatov, V. A.; O'Keeffe, M.; Proserpio, D. M. Vertex-, Face-, Point-, Schläfli-, and Delaney-Symbols in Nets, Polyhedra and Tilings: Recommended Terminology. *CrystEngComm* **2010**, *12* (1), 44.

(42) Essam, J. W.; Fisher, M. E. Some Basic Definitions in Graph Theory. *Rev. Mod. Phys.* **1970**, *42* (2), 272–288.

(43) Blatov, V. A.; Delgado-Friedrichs, O.; O'Keeffe, M.; Proserpio, D. M. Three-Periodic Nets and Tilings: Natural Tilings for Nets. *Acta Crystallogr. A.* **2007**, *63* (Pt 5), 418–425.

(44) Slater, J. C. Atomic Radii in Crystals. *J. Chem. Phys.* **1964**, *41* (10), 3199.

(45) Desgranges, L.; Baldinozzi, G.; Rousseau, G.; Nièpce, J.-C.; Calvarin, G. Neutron Diffraction Study of the in Situ Oxidation of UO(2). *Inorg. Chem.* **2009**, *48*, 7585–7592.

(46) Belin, R. C.; Valenza, P. J.; Reynaud, M. A.; Raison, P. E. New Hermetic Sample Holder for Radioactive Materials Fitting to Siemens D5000 and Bruker D8 X-Ray Diffractometers: Application to the Rietveld Analysis of Plutonium Dioxide. *J. Appl. Crystallogr.* **2004**, *37* (6), 1034–1037.

(47) Taggard Jr, J. E.; Foord, E. E.; Rosenzweig, A.; Hanson, T. Scrutinyite, Natural Occurrence of A-PbO2from Bingham, New Mexico, U.S.A., and Mapimi, Mexico. *Can. Mineral.* **1988**, *26*, 905–910.

(48) Kolitsch, U.; Maczka, M.; Hanuza, J. NaAl(MoO4)2: A Rare Structure Type among Layered Yavapaiite-Related AM(XO4)2 Compounds. *Acta Crystallogr. Sect. E Struct. Reports Online* **2003**, *59* (2), i10–i13.

(49) Sozzani, P.; Bracco, S.; Comotti, A.; Ferretti, L.; Simonutti, R. Methane and Carbon Dioxide Storage in a Porous van Der Waals Crystal. *Angew. Chem. Int. Ed. Engl.* **2005**, *44* (12), 1816–1820.

(50) Michel, C.; Groult, D.; Deschanvres, A.; Raveau, B. Proprietes D'echange D'ions Des Pyrochlores AB2O6—II Evolution Thermique Des Pyrochlores AMWO6.H2O (A = Li, Na, Ag; M = Nb, Ta, Sb). *Journal of Inorganic and Nuclear Chemistry*, 1975, *37*, 251–255.

(51) Knyazev, A. V.; Mączka, M.; Smirnova, N. N.; Macalik, L.; Kuznetsova, N. Y.; Letyanina, I. A. Crystal Structure, Spectroscopy and Thermodynamic Properties of MIVWO6(MI – Li, Na). *J. Solid State Chem.*, **2009**, *182*, 3003–3012.

(52) Berdonosov, P. S.; Charkin, D. O.; Knight, K. S.; Johnston, K. E.; Goff, R. J.; Dolgikh, V. A.; Lightfoot, P. Phase Relations and Crystal Structures in the Systems (Bi,Ln)2WO6 and (Bi,Ln)2MoO6 (Ln=lanthanide). *J. Solid State Chem.* **2006**, *179*, 3437–3444.

(53) Macalik, L.; Tomaszewski, P. E.; Lisiecki, R.; Hanuza, J. The Crystal Structure, Vibrational and Luminescence Properties of the Nanocrystalline KEu(WO4)2 and KGd(WO4)2:Eu3+ Obtained by the Pechini Method. *J. Solid State Chem.*, **2008**, *181*, 2591–2600.

(54) Fu, W. T.; Au, Y. S.; Akerboom, S.; IJdo, D. J. W. Crystal Structures and Chemistry of Double Perovskites Ba2M(II)M???(VI)O6 (M=Ca, Sr, M???=Te, W, U). *J. Solid State Chem.* **2008**, *181*, 2523–2529.

(55) Krut'ko, V. A.; Belik, A. A.; Lysanova, G. V. Structures of Nonlinear Hexagonal Boratotungstates Ln3 B WO9 (Ln= La, Pr, Nd, Sm, Gd, Tb, Dy). *Zhurnal Neorg. Khimii* **2006**, *51* (6), 954–959.

(56) Hong, S. T. Novel Perovskite-Related Barium Tungstate Ba11W4O23. *J. Solid State Chem.* **2007**, *180*, 3039–3048.

(57) Lv, P.; Chen, D.; Li, W.; Xue, L.; Huang, F.; Liang, J. Subsolidus Phase Relationships in the System ZnO-Li2O-WO3. *J. Alloys Compd.* **2008**, *460*, 142–146.

(58) Jiang, H. L.; En, M.; Mao, J. G. New Luminescent Solids in the Ln-W(Mo)-Te-O-(Cl) Systems. *Inorg. Chem.* **2007**, *46* (17), 7012–7023.

(59) Brixner, L. H.; Chen, H. -y.; Foris, C. M. Structure and Luminescence of the Monoclinic LnWO4Cl-Type Rare Earth Halo Tungstates. *Mater. Res. Bull.* **1982**, *17*, 1545–1556.

(60) Boulahya, K.; Parras, M.; González-Calbet, J. M. A Structural Study of the Solid Solution Eu2(Mo1-xWx)3O12. *Z. Anorg. Allg. Chem.* **2005**, *631*, 1988–1990.

(61) Bang Jin, G.; Soderholm, L. Syntheses and Single-Crystal Structures of CsTh(MoO4)2Cl and Na4Th(WO4)4. *J. Solid State Chem.* **2011**, *184*, 337–342.

(62) Efremov, V. A.; Berezina, T. A.; Averina, I. M.; Trunov, V. K. Structure of Na5 Tb (Mo O4)4, Na5 Lu (Mo O4)4, and Na5 Lu (W O4)4. *Kristallografiya* **1980**, *25*, 254–261.

(63) Efremov, V. A.; Trunov, V. K.; Berezina, T. A. Fine Changes in the Structure of Scheelite-like Na5 Tr (E O4)4 with a Variation in Their Elemental Composition. *Kristallografiya* **1982**, *27*, 134–139.

(64) Grivel, J. C.; Norby, P. Subsolidus Phase Relations of the SrO-WO3-CuO System at 800° C in Air. *J. Alloys Compd.* **2012**, *513*, 304–309.

(65) Manjón, F. J.; López-Solano, J.; Ray, S.; Gomis, O.; Santamaría-Pérez, D.; Mollar, M.; Panchal, V.; Errandonea, D.; Rodríguez-Hernández, P.; Muñoz, A. High-Pressure Structural and Lattice Dynamical Study of HgWO4. *Phys. Rev. B - Condens. Matter Mater. Phys.* **2010**, *82*, 035212–1 – 035212–12.

(66) Klug, A. X-Ray Diffraction Studies of Potassium Polytungstates with High WO3 Content. *Mater. Res. Bull.*, **1977**, *12*, 837–845.

(67) Okada, K.; Marumo, F.; Iwai, S. The Crystal Structure of K2W4O13. *Acta Crystallogr. Sect. B Struct. Crystallogr. Cryst. Chem.* **1978**, *34*, 3193–3195.

(68) Mormann, T. J.; Jeitschko, W. Mercury(I) Molybdates and Tungstates: Hg2WO4 and Two Modifications of Hg2MoO4. *Inorg. Chem.* **2000**, *39*, 4219–4223.

(69) Kovba, L. M.; Lykova, L. N.; Balashov, V. L.; Kharlanov, A. L. Crystal Structure of Ba2WO5. *Koord. Khimiya* **1985**, *11* (10), 1426–1429.

(70) Guarnieri, A. A.; Moreira, A. M.; Pinheiro, C. B.; Speziali, N. L. Structural and Calorimetric Studies of Mixed K2MoxW(1−x)O4 (0⩽x⩽1) Compounds. *Physica B: Condens. Matter*, **2003**, *334*, 303–309.

(71) Okada, K.; Morikawa, H.; Marumo, F.; Iwai, S. The Crystal Structure of Li2W2O7. *Acta Crystallogr. Sect. B Struct. Crystallogr. Cryst. Chem.* **1975**, *31*, 1451–1454.

(72) Li, Y.-Y.; Cheng, W.-D.; Zhang, H.; Lin, C.-S.; Zhang, W.-L.; Geng, L.; Chai, G.-L.; Luo, Z.-Z.; He, Z.-Z. A Series of Novel Rare-Earth Bismuth Tungstate Compounds LnBiW2O9 (Ln=Ce, Sm, Eu, Er): Synthesis, Crystal Structure, Optical and Electronic Properties. *Dalton Trans.* **2011**, *40*, 7357–7364.

(73) Hartenbach, I.; Schleid, T. Na3F[WO4]: A Sodium FluorideOrtho-Oxotungstate(VI) with Strands of Face-Shared Fluoride-Centred Sodium Octahedra According to. *Z. Anorg. Allg. Chem.* **2007**, *633*, 524–526.

(74) Hartenbach, I.; Marchetti, B.; Schleid, T. Na5Y[WO4]4: Ein Natrium - Yttrium - Ortho-Oxowolframat Mit Einer Teraedrischen Na+ - Koordination. *Z. Kristallogr. Suppl. Issue* **2007**, *25* (079), 22.

(75) Sundberg, M.; Marinder, B. Ordered and Defect Structures in the UO2 – WO3 System, Revealed by HREM. *J. Solid State Chem.* **1996**, *121*, 167–173.

(76) Marinder, B. O.; Wang, P.-L.; Werner, P. E.; Westdahl, M.; Andresen, A. F.; Louer, D. Powder Diffraction Studies of Cu2WO4. *Acta Chem. Scand. Ser. A* **1987**, *41*, 152–157.

(77) Grice, J. D.; Dunn, P. J. Crystal Structure Determination of Pinalite. *Am. Mineral.* **2000**, *85*, 806–809.

(78) Müller-Buschbaum, H.; Gressling, T. Zur Dimorphie von Kupfer-Lanthanoid-Oxowolframaten Am Beispiel von CuErW2O8, Mit Einem Beitrag Über CuDyW2O8. *J. Alloys Compd.* **1993**, *202*, 63–67.

(79) Boehlke, A.; Müller-Buschbaum, H. Ein Beitrag Zur Kristallstruktur von CuLaW2O8 Und CuSmW2O8. *J. Less Common Met.* **1990**, *162*, 141–147.

(80) Okada, K.; Ossaka, J.; Iwai, S. Structure of Dithallium tungstate(VI). *Acta Crystallogr. Sect. B Struct. Crystallogr. Cryst. Chem.* **1979**, *35*, 2189–2191.

(81) Barker, R. S.; Evans, I. R. Structural Characterization of RE10W22O81 Rare-Earth Tungstates (RE = Ce, Nd). *Acta Crystallogr. Sect. B Struct. Sci.* **2008**, *64*, 708–712.

(82) Mumm, H.-C.; Müller-Buschbaum, H. Zur Kristallstruktur von Cu2WO4. *J. Less Common Met.* **1988**, *142*, 85–90.

(83) Gressling, T.; Müller-Buschbaum, H. Ein Neuer Strukturtyp Am Lanthanoid-Oxowolframat FeCe(WO4)W2O8 = FeCe(WO4)3. *Z. Anorg. Allg. Chem.* **1996**, *622*, 254–258.

(84) Sundberg, M.; Lundberg, M. Kx(Nb,W)17O47 (1LxL2): A New Tunnel Structure Derived from High-Resolution Electron Micrographs. *Acta Crystallogr. Sect. B Struct. Sci.* **1987**, *43*, 429–434.

(85) Hanuza, J.; Maczka, M.; Hermanowicz, K.; Andruszkiewicz, M.; Pietraszko, A.; Strek, W.; Dereń, P. The Structure and Spectroscopic Properties of Al2-xCrx(WO4)3 Crystals in Orthorhombic and Monoclinic Phases. *J. Solid State Chem.* **1993**, *105*, 49–69.

(86) Woodcock, D. A.; Lightfoot, P.; Ritter, C. Negative Thermal Expansion in Y2(WO4)3. *J. Solid State Chem.* **2000**, *149*, 92–98.

(87) Chan, L. Y. Y.; Geller, S. Crystal Structure and Conductivity of 26-Silver 18-Iodide Tetratungstate, Ag26I18W4O16. *J. Solid State Chem.* **1977**, *21*, 331–347.

(88) Evans, J. S. O.; Mary, T. A.; Vogt, T.; Subramanian, M. A.; Sleight, A. W. Negative Thermal Expansion in ZrW2O8 and HfW2O8. *Chem. Mat.* **1996**, *8*, 2809–2823.

(89) Spitsyn, V. I.; Balashov, V. L.; Kharlanov, A. L.; Lykova, L. N.; Kovba, L. M. Crystal Structure of Ba3WO5Cl2. *Dokl. Akad. Nauk SSSR* **1985**, *284* (1), 125–127.

(90) Tyulin, A. V.; Efremov, V. A. Polymorphism of Oxytungstates Tr2WO6. Mechanism of Structural Changes of Er2 W O6. *Kristallografiya* **1987**, *32*, 363–370.

(91) Tyulin, A. V.; Efremov, V. A.; Trunov, V. K. Polymorphism of Oxytungstates TR2WO6. Mechanisms of Structural Changes in Y2WO6. *Kristallografiya* **1989**, *34*, 885–892.

(92) Tyulin, A. V.; Efremov, V. A. Polymorphism of Oxytungstates Tr2WO6. Analysis of Structural Type II (Gd2WO6 and Gd2MoO6). Mechanism of Structural Change in Gd2 W O6 in the Phase Transition II <-> V. *Kristallografiya* **1987**, *32*, 371–377.

(93) Farrugia, L. J. Sodium Tungstate Dihydrate: A Redetermination. *Acta Crystallogr. Sect. E Struct. Reports Online* **2007**, *63*.

(94) Ewing, R. C. Nuclear Waste Forms for Actinides. *Proc. Natl. Acad. Sci. U. S. A.* **1999**, *96* (7), 3432–3439.

(95) Pujol, M. C.; Mateos, X.; Aznar, A.; Solans, X.; Suriñach, S.; Massons, J.; Díaz, F.; Aguiló, M. Structural Redetermination, Thermal Expansion and Refractive Indices of KLu(WO4)2. *J. Appl. Crystallogr.* **2006**, *39*, 230–236.

(96) Pujol, M. C.; Mateos, X.; Solé, R.; Massons, J.; Gavaldà, J.; Solans, X.; Díaz, F.; Aguiló, M. Structure, Crystal Growth and Physical Anisotropy of KYb(WO4)2, a New Laser Matrix. *J. Appl. Crystallogr.* **2002**, *35*, 108–112.

(97) Borowiec, M. T.; Dyakonov, V. P.; Woźniak, K.; Dobrzycki, Ł.; Berkowski, M.; Zubov, E. E.; Michalski, E.; Szewczyk, A.; Gutowska, M. U.; Zayarnyuk, T.; et al. Crystal Structure and Magnetic Properties of Potassium Erbium Double Tungstate KEr(WO 4) 2. *J. Phys. Condens. Matter* **2007**, *19*, 056206.

(98) Gallucci, E.; Goutaudier, C.; Boulon, G.; Cohen-Adad, M. T.; Mentzen, B. F. Nonstoichiometric KY(WO4)2: Crystal Growth, Chemical and Physical Characterization. *J. Cryst. Growth* **2000**, *209*, 895–905.

(99) Borowiec, M. T.; Dyakonov, V. P.; Wozniak, K.; Dobrzycki, L.; Majchrowski, A.; Michalski, E.; Zubov, E. E.; Khatsko, E. N.; Zayarnyuk, T.; Szewczyk, A.; et al. Crystalline Structure of Potassium Holmium Double Tungstate. *Acta Phys. Pol. A* **2011**, *119* (6), 835–837.

(100) Gateshki, M.; Igartua, J. M. Second-Order Structural Phase Transition in Sr2CuWO6 Double-Perovskite Oxide. *J. Phys. Condens. Matter* **2003**, *15*, 6749–6757.

(101) Alvarez-Vega, M.; Rodriguez-Carvajal, J.; Reyes-Cardenas, J. G.; Fuentes, A. F.; Amador, U. Synthesis and Characterization of New Double Tungstates Li2MII(WO4)2 (M = Co, Ni, and Cu). *Chem. Mater.* **2001**, *13*, 3871–3875.

(102) McDowell, N. A.; Knight, K. S.; Lightfoot, P. Unusual High-Temperature Structural Behaviour in Ferroelectric Bi2WO6. *Chem. - A Eur. J.* **2006**, *12*, 1493–1499.

(103) Shen, R.; Wang, C.; Wang, T. M.; Dong, C.; Chen, X. L.; Liang, J. K. Crystal Structures of Dy2(WO4)3 and GdY(WO4)3. *Rare Met.* **2003**, *22* (1), 49–54.

(104) Templeton, D. H.; Zalkin, A. Crystal Structure of Europium Tungstate. *Acta Crystallogr.* **1963**, *16*, 762–766.

(105) Polyanskaya, T. M.; Borisov, S. V.; Belov, N. V. The Crystal Structure of Pr3WO6Cl3. *Dokl. Akad. Nauk SSSR* **1969**, *187*, 1043–1046.

(106) Parise, J. B.; Brixner, L. H.; Prince, E. Refinement of the Structure of Trilanthanum Trichlorohexaoxotungstate, La3WO6Cl3, from Neutron Powder Diffraction Data. *Acta Crystallogr. Sect. C Cryst. Struct. Commun.* **1983**, *39*, 1326–1328.

(107) Michel, C.; Guyomarc'h, A.; Raveau, B. Nouveaux Echangeurs Cationiques Avec Une Structure a Tunnels Entrecroises: Les Oxydes A12M33O90 et A12M33O90, 12H2O. *J. Solid State Chem.* **1977**, *22*, 393–403.

(108) Kim, J. S.; Lee, J. C.; Cheon, C. Il; Kang, H. J. Crystal Structures and Low Temperature Cofiring Ceramic Property of (1 - X)(Li, RE)W2O8-xBaWO4 Ceramics (RE = Y, Yb). *Japanese J. Appl. Physics, Part 1 Regul. Pap. Short Notes Rev. Pap.* **2006**, *45*, 7397–7400.

(109) Kondo, R. The Synthesis and Crystallography of a Group of New Compounds Belonging to the Hauyne Type Structure. *J. Ceram. Assoc. Japan* **1965**, *73*, 1–8.

(110) Müller-Buschbaum, H.; Sedello, O. Die Kristallstrukturen von A-CuGdW2O8 Und CuNdMo2O8. *J. Alloys Compd.* **1994**, *204*, 237–241.

(111) Klevtsova, R. F.; Kharchenko, L. Y.; Borisov, S. V.; Efremov, V. A.; Klevtsov, P. V. Triclinic Modification of Lithium-Rare Earth Tungstates Li Ln (W O4)2, Where Ln Is La-Sm. *Kristallografiya* **1979**, *24*, 446–454.

(112) Gressling, T.; Müller-Buschbaum, H. Ein Neuer Strukturtyp Bei Kupfer-Lanthanoid-Oxowolframaten: CuDy5(WO4)8. *Z. Anorg. Allg. Chem.* **1995**, *621*, 181–185.

(113) Shigematsu, H.; Nomura, K.; Nishiyama, K.; Tojo, T.; Kawaji, H.; Atake, T.; Kawamura, Y.; Miyoshi, T.; Matsushita, Y.; Tanaka, M.; et al. Structures and Phase Transitions in Rb 2 MoO 4 and Rb 2 WO 4. *Ferroelectrics* **2011**, *414*, 195–200.

(114) Chang, H. Y.; Sivakumar, T.; Ok, K. M.; Shiv Halasyamani, P. Polar Hexagonal Tungsten Bronze-Type Oxides: KNbW2O9, RbNbW2O9, and KTaW2O9. *Inorg. Chem.* **2008**, *47*, 8511–8517.

(115) Rozanova, O. N.; Pol'shchikova, Z. Y.; Kovba, L. M. Crystal Structure of Uranium Tungstate U (W O4)2. *Radiokhimiya* **1978**, *20*, 125–127.

(116) Singh, D. J. Relationship of Li2 W O4 to the Scheelite Tungstate Scintillators: Electronic Structure and Atomic Positions from Density-Functional Calculations. *Phys. Rev. B - Condens. Matter Mater. Phys.* **2008**, *77*, 113101.

(117) Zachariasen, W. H.; Plettinger, H. A. The Crystal Structure of Lithium Tungstate. *Acta Crystallogr.* **1961**, *14*, 229–230.

(118) Abrahams, S. C.; Bernstein, J. L. Crystal Structure of the Transition-Metal Molybdates and Tungstates. II. Diamagnetic Sc2(WO4)3. *J. Chem. Phys.* **1966**, *45*, 2745–2752.

(119) Richard, A. P.; Edwards, D. D. Subsolidus Phase Relations and Crystal Structures of the Mixed-Oxide Phases in the In2O3-WO3 System. *J. Solid State Chem.* **2004**, *177*, 2740–2748.

(120) Lamire, M.; Labbé, P.; Goreaud, M.; Raveau, B. Ba2P8W32O112: Structural Study in Comparison with the K and Rb Diphosphate Tungsten Bronzes with Hexagonal Tunnels. *J. Solid State Chem.* **1987**, *71*, 342–348.

(121) Chakraborty, K. R.; Das, A.; Krishna, P. S. R.; Yusuf, S. M.; Patwe, S. J.; Achary, S. N.; Tyagi, A. K. A Low Temperature Magnetization and Neutron Diffraction Study of Ca2NiWO6. *J. Alloys Compd.* **2008**, *457*, 15–18.

(122) Horiuchi, H.; Morimoto, N.; Yamaoka, S. The Crystal Structure of Li2WO4II: A Structure Related to Spinel. *J. Solid State Chem.* **1979**, *30*, 129–135.

(123) Depmeier, W.; Yamamoto, A. Powder Profile Refinement of a Commensurately Modulated Aluminate Sodalite. *Mater. Sci. Forum* **1991**, *79-82*, 763–768.

(124) Champarnaud-Mesjard, J.-C.; Frit, B.; Watanabe, A. Crystal Structure of Bi2W2O9, the n=2 Member of the Homologous Series (Bi2O2)BVInO3n+1 of Cation-Deficient Aurivillius Phases. *J. Mater. Chem.* **1999**, *9*, 1319–1322.

(125) Jorgensen, J.; Hu, Z.; Teslic, S.; Argyriou, D.; Short, S.; Evans, J.; Sleight, A. Pressure-Induced Cubic-to-Orthorhombic Phase Transition in ZrW2O8. *Phys. Rev. B* **1999**, *59*, 215–225.

(126) Okada, K.; Ossaka, J. Caesium Lithium Tungstate: A Stuffed H-Cristobalite Structure. *Acta Crystallogr. Sect. B Struct. Crystallogr. Cryst. Chem.* **1980**, *36*, 657–659.

(127) Wang, K.; Zhang, J.; Wang, J.; Yu, W.; Zhang, H.; Wang, X.; Wang, Z.; Ba, M. Growth, Structure and Morphology Study of Monoclinic RbGd(WO 4)2 Crystals. *J. Cryst. Growth* **2005**, *281*, 407–410.

(128) Xie, H.; Shen, D.; Xie, C.; Wang, X.; Shen, G. Crystal Growth and Structure of KBi(WO4)2 Single Crystals. *Cryst. Res. Technol.* **2006**, *41*, 961–966.

(129) Borowiec, M. T.; Prokhorov, A. D.; Krygin, I. M.; Dyakonov, V. P.; Woźniak, K.; Dobrzycki; Zayarnyuk, T.; Barański, M.; Domuchowski, W.; Szymczak, H. Crystal Structure and EPR of the RbNd(WO4)2 Single Crystal. *Phys. B Condens. Matter* **2006**, *371*, 205–209.

(130) Obbade, S.; Dion, C.; Bekaert, E.; Yagoubi, S.; Saadi, M.; Abraham, F. Synthesis and Crystal Structure of New Uranyl Tungstates M2(UO2)(W2O8) (M=Na, K), M2(UO2)2(WO5)O (M=K, Rb), and Na10(UO2)8(W5O20)O8. *J. Solid State Chem.* **2003**, *172*, 305–318.

(131) Obbade, S.; Yagoubi, S.; Dion, C.; Saadi, M.; Abraham, F. Two New Lithium Uranyl Tungstates Li2(UO2)(WO 4)2 and Li2(UO2)4(WO 4)4O with Framework Based on the Uranophane Sheet Anion Topology. *J. Solid State Chem.* **2004**, *177*, 1681–1694.

(132) Horiuchi, H.; Morimoto, N.; Yamaoka, S. The Crystal Structure of Li2WO4(IV) and Its Relation to the Wolframite-Type Structure. *J. Solid State Chem.* **1980**, *33*, 115–119.

(133) Huang, J.; Xu, J.; Li, H.; Luo, H.; Yu, X.; Li, Y. Determining the Structure of Tetragonal Y2WO6 and the Site Occupation of Eu3 Dopant. *J. Solid State Chem.* **2011**, *184* (4), 843–847.

(134) Stomberg, R. Structure of Potassium tetraperoxotungstate(VI), K2[W(O2)4]. *J. Less Common Met.* **1988**, *143*, 363–371.

(135) Depmeier, W. Structure of Cubic Aluminate Sodalite Ca8[Al12O24](WO4)2 in Comparison with Its Orthorhombic Phase and with Cubic Sr8[Al12O24](CrO4)2. *Acta Crystallogr. Sect. B Struct. Sci.* **1988**, *44*, 201–207.

(136) Knight, K. S. The Crystal Structure of Russellite; a Re-Determination Using Neutron Powder Diffraction of Synthetic Bi2WO6. *Mineral. Mag.* **1992**, *56*, 399–409.

(137) Gärtner, M.; Abeln, D.; Pring, A.; Wilde, M.; Reller, A. Synthesis, Structure, and Reactivity of Novel Lanthanum Tungstates. *J. Solid State Chem.* **1994**, *111*, 128–133.

(138) Jeannin, Y.; Launay, J. P.; Sedjadi, M. A. S. Crystal and Molecular Structure of the Six-Electron-Reduced Form of Metatungstate Rb4H8[H2W12O40](H2O)18: Occurrence of a Metal-Metal Bonded Subcluster in a Heteropolyanion Framework. *Inorg. Chem.* **1980**, *19*, 2933–2935.

(139) Fourquet, J. L.; Le Bail, A.; Gillet, P. A. LiNbWO6: Crystal Structure of Its Two Allotropic Forms. *Mater. Res. Bull.* **1988**, *23*, 1163–1170.

(140) Knyazev, A. V.; McZka, M.; Kuznetsova, N. Y. Thermodynamic Modeling, Structural and Spectroscopic Studies of the KNbWO6-KSbWO6-KTaWO6 System. *Thermochim. Acta* **2010**, *506*, 20–27.

(141) Knyazev, A. V.; Kuznetsova, N. Y. Crystal Structure of Compounds CsAVA′VIO6 (AV = Sb, Ta; A′VI = W, U). *Radiochemistry* **2009**, *51*, 1–4.

(142) Murphy, D.; Cava, R.; Rhyne, K.; Roth, R.; Santoro, A.; Zahurak, S.; Dye, J. Structural Aspects of Insertion Reactions of the Pyrochlore, KNbWO6. *Solid State Ionics* **1986**, *18-19*, 799–801.

(143) Pakhomov, V. I.; Fedorov, P. M.; Okunera, A. S.; Sorokina, O. V. Structure and Elastic Properties of AgIn(WO4)2. *Koord. Khimiya* **1977**, *3*, 765–767.

(144) Postema, J. M.; Fu, W. T.; Ijdo, D. J. W. Crystal Structure of LiLnW2O8 (Ln=lanthanides and Y): An X-Ray Powder Diffraction Study. *J. Solid State Chem.* **2011**, *184* (8), 2004–2008.

(145) Tyagi, M.; Singh, S. G.; Sangeeta; Prasad, R.; Auluck, S.; Singh, D. J. A Study of Electronic and Optical Properties of NaBi(WO4)2: A Disordered Double Tungstate Crystal. *Phys. B Condens. Matter* **2010**, *405*, 3267–3271.

(146) Bonin, M.; Paciorek, W.; Schenk, K. J.; Chapuis, G. X-Ray Study of and Structural Approach to the Incommensurate Perovskite Pb2CoWO6. *Acta Crystallogr. Sect. B Struct. Sci.* **1995**, *51*, 48–54.

(147) Zhengmin, F.; Wenxiu, L. Crystal Structure of the High-Temperature Phase of a Compound Sr2ZnWO6. *Powder Diffr.* **1992**, *7*, 226–227.

(148) Patwe, S. J.; Achary, S. N.; Mathews, M. D.; Tyagi, A. K. Synthesis, Phase Transition and Thermal Expansion Studies on M2MgWO6 (M = Ba2+ and Sr2+) Double Perovskites. *J. Alloys Compd.* **2005**, *390*, 100–105.

(149) Martínez-Lope, M. J.; Alonso, J. A.; Casais, M. T.; Fernández-Díaz, M. T. Preparation, Crystal and Magnetic Structure of the Double Perovskites Ba2CoBO6 (B = Mo, W). *Eur. J. Inorg. Chem.* **2002**, *2002*, 2463–2469.

(150) Cox, D. E.; Shirane, G.; Frazer, B. C. Neutron-Diffraction Study of Antiferromagnetic Ba2CoWO6 and Ba2NiWo6. *J. Appl. Phys.* **1967**, *38*, 1459–1460.

(151) Azad, A. K.; Eriksson, S.-G.; Mellergård, A.; Ivanov, S. A.; Eriksen, J.; Rundlöf, H. A Study on the Nuclear and Magnetic Structure of the Double Perovskites A2FeWO6 (A = Sr, Ba) by Neutron Powder Diffraction and Reverse Monte Carlo Modeling. *Mater. Res. Bull.* **2002**, *37*, 1797–1813.

(152) Baldinozzi, G.; Sciau, P.; Buffat, P.-A. Investigation of the Orthorhombic Structures of Pb2MgWO6 and Pb2CoWO6. *Solid State Commun.* **1993**, *86* (9), 541–544.

(153) Bugaris, D. E.; Hodges, J. P.; Huq, A.; zur Loye, H.-C. Crystal Growth, Structures, and Optical Properties of the Cubic Double Perovskites Ba2MgWO6 and Ba2ZnWO6. *J. Solid State Chem.* **2011**, *184* (8), 2293–2298.

(154) Fu, W. T.; Akerboom, S.; IJdo, D. J. W. Crystal Structures of the Double Perovskites Ba2Sr1-xCaxWO6. *J. Solid State Chem.* **2007**, *180* (5), 1547–1552.

(155) Klevtsov, P. V.; Klevtsova, R. F. Single-Crystal Synthesis and Investigation of the Double Tungstates NaR3+(WO4)2, Where R3+ = Fe, Sc, Ga, and In. *J. Solid State Chem.* **1970**, *2*, 278–282.

(156) Keeling, R. O. The Structure of NiWO4. *Acta Crystallogr.* **1957**, *10*, 209–213.

(157) Shimony, Y.; Ben-Dor, L. On the Crystal Structure of CrWO4. *Mater. Res. Bull.* **1983**, *18*, 331–335.

(158) Errandonea, D.; Pellicer-Porres, J.; Manjón, F. J.; Segura, A.; Ferrer-Roca, C.; Kumar, R. S.; Tschauner, O.; Rodríguez-Hernández, P.; López-Solano, J.; Radescu, S.; et al. High-Pressure Structural Study of the Scheelite Tungstates CaWO4 and SrWO4. *Phys. Rev. B - Condens. Matter Mater. Phys.* **2005**, *72*, 174106.

(159) Velikodnyi, Y. A.; Trunov, V. K. Structure of the Double Wolframate Na In (W O4)2. *Zhurnal Strukt. Khimii* **1971**, *12*, 334.

(160) Errandonea, D.; Pellicer-Porres, J.; Manjón, F. J.; Segura, A.; Ferrer-Roca, C.; Kumar, R. S.; Tschauner, O.; López-Solano, J.; Rodríguez-Hernández, P.; Radescu, S.; et al. Determination of the High-Pressure Crystal Structure of BaWO4 and PbWO4. *Phys. Rev. B - Condens. Matter Mater. Phys.* **2006**, *73*, 224103.

(161) Baldinozzi, G.; Sciau, P.; Lapasset, J. Crystal Structure of Pb2CoWO6 in the Cubic Phase. *Phys. Status Solidi* **1992**, *133*, 17–23.

(162) Becka, L. N.; Poljak, R. . Estructura Cristalina Del MoO4Na2 Y Del WO4Na2. *An. la Asoc. Quim. Argentina* **1958**, *46*, 204–209.

(163) Cheviré, F.; Tessier, F.; Marchand, R. New Scheelite-Type Oxynitrides in Systems RWO3N-AWO4 (R = Rare-Earth Element; A = Ca, Sr) from Precursors Obtained by the Citrate Route. *Mater. Res. Bull.* **2004**, *39*, 1091–1101.

(164) Zhao, D.; Li, F.; Cheng, W.; Zhang, H. Scheelite-Type NaDy(WO4)2. *Acta Crystallogr. Sect. E Struct. Reports Online* **2010**, *66*.

(165) Hanuza, J.; Benzar, A.; Haznar, A.; Maczka, M.; Pietraszko, A.; Van Der Maas, J. H. Structure and Vibrational Dynamics of Tetragonal NaBi(WO4)2 Scheelite Crystal. *Vib. Spectrosc.* **1996**, *12*, 25–36.

(166) Li, H.; Hong, G.; Yue, S. Crystal Study of NaLn(WO4)2 (Ln= La, Pr, Nd). *Zhongguo Xitu Xuebao* **1990**, *8*, 37–41.

(167) Perets, S.; Tseitlin, M.; Shneck, R. Z.; Mogilyanski, D.; Kimmel, G.; Burshtein, Z. Sodium Gadolinium Tungstate NaGd(WO4)2: Growth, Crystallography, and Some Physical Properties. *J. Cryst. Growth* **2007**, *305*, 257–264.

(168) Xu, K.-Q.; Xue, J.-Y.; Ding, Y.; Lu, G.-G. Discovery of Stolzite in China and Refinement of Its Crystal Structure. *Dizhi Xuebao* **1994**, *68*, 287–292.

(169) De Moraes, J. R.; Baldochi, S. L.; Soares, L. dos R. L.; Mazzocchi, V. L.; Parente, C. B. R.; Courrol, L. C. Growth, Structural and Optical Characterizations of LiLa(1−x)Eux(WO4)2 Single-Crystalline Fibers by the Micro-Pulling-down Method. *Mater. Res. Bull.* **2012**, *47*, 744–749.

(170) Klevtsova, R. F.; Bakakin, V. V.; Solodovnikov, S. F.; Glinskaya, L. A. The Combination of the Wolframite's and Scheelite's Motives in the Crystal Structure of Sodium and Zirconium Tungstate Na2ZrW3O12 = Na2ZrW2O8(WO4). *Zhurnal Strukt. Khimii* **1981**, *22*, 6–11.

(171) Gokhman, L. Z.; Dzhurinskii, B. F.; Efremov, V. A.; Ilyukhin, A. B.; Chistova, V. I. Synthesis and Structure of Boratotungstates Ln3 B W O9 (Ln= La, Pr, Nd, Sm-Ho). *Zhurnal Neorg. Khimii* **1994**, *39*, 1075–1079.

(172) Han, X.; Lin, Z.; Hu, Z.; Wang, G. Structure of KLa(WO4)2 with a Novel Isolated La Polyhedron. *Mater. Res. Innov.* **2002**, *6*, 118–121.

(173) Torardi, C. C.; Page, C.; Brixner, L. H.; Blasse, G.; Dirksen, G. J. Structure and Luminescence of Some CsLnW2O8 Compounds. *J. Solid State Chem.* **1987**, *69*, 171–178.

(174) Ra, H. S.; Ok, K. M.; Halasyamani, P. S. Combining Second-Order Jahn-Teller Distorted Cations to Create Highly Efficient SHG Materials: Synthesis, Characterization, and NLO Properties of BaTeM2O9 (M = Mo6+ or W6+). *J. Am. Chem. Soc.* **2003**, *125*, 7764–7765.

(175) Mączka, M.; Tomaszewski, P.; Stępień-Damm, J.; Majchrowski, A.; Macalik, L.; Hanuza, J. Crystal Structure and Vibrational Properties of Nonlinear Eu3BWO9 and Nd3BWO9 Crystals. *J. Solid State Chem.* **2004**, *177*, 3595–3602.

(176) Goodey, J.; Ok, K. M.; Broussard, J.; Hofmann, C.; Escobedo, F. V.; Halasyamani, P. S. Syntheses, Structures, and Second-Harmonic Generating Properties in New Quaternary Tellurites: A2TeW3O12 (A=K, Rb, or Cs). *J. Solid State Chem.* **2003**, *175*, 3–12.

(177) Range, K.-J.; Klement, U.; Rau, F.; Schiessl, U.; Heyns, A. M. Crystal Structure of Rubidium ditungstate(VI), Rb 2 W 2 O 7. *Z. Kristallogr.* **1993**, *203*, 318–319.

(178) Moutou, J. M.; Vlasse, M.; Cervera-Marzal, M.; Chaminade, J. P.; Pouchard, M. A Structural Study of a New Lithium Oxyfluorotungstate, LiW3O9F. *J. Solid State Chem.* **1984**, *51*, 190–195.

(179) Hong, H. .-P.; Dwight, K. Crystal Structure and Fluorescence Lifetime of a Laser Material NdNa5(WO4)4. *Mater. Res. Bull.* **1974**, *9*, 775–780.

(180) Klevtsova, R. F.; Volkova, L. M. Crystal Structure of Monoclinic K Nd (W O4)2. *Kristallografiya* **1972**, *17*, 859–861.

(181) Zikmund, Z. The Crystal Structure of Ca3WO6Cl2 and the Configuration of the WO54− Ion. *Acta Crystallogr. Sect. B Struct. Crystallogr. Cryst. Chem.* **1974**, *30*, 2587–2593.

(182) Klevtsova, R. F.; Borisov, S. V. The Crystal Structure of NdWO4(OH). *Kristallografiya* **1969**, *14*, 904–907.

(183) Li, J.; Pan, S.; Zhao, W.; Tian, X.; Han, J.; Fan, X. Synthesis and Crystal Structure of a Novel Boratotungstate: Pb6B2WO12. *Solid State Sci.* **2011**, *13*, 966–969.

(184) Bruedgam, I.; Fuchs, J.; Hartl, H.; Palm, R. Two New isopolyoxotungstates(VI) with the Empirical Composition Cs2W2O7 * 2(H2O) and Na2W2O7 * H2O: A Icosatetratungstate and a Polymeric Compound. *Angew. Chemie. Int. Ed.* **1998**, *37*, 2668–2671.

(185) Meredig, B.; Wolverton, C. A Hybrid Computational-Experimental Approach for Automated Crystal Structure Solution. *Nat. Mater.* **2013**, *12*, 123–127.

(186) Yang, L.; Dacek, S.; Ceder, G. Proposed Definition of Crystal Substructure and Substructural Similarity. *Phys. Rev. B - Condens. Matter Mater. Phys.* **2014**, *90* (5), 1–9.

(187) Fuchs, A. H.; Cheetham, A. K. Adsorption of Guest Molecules in Zeolitic Materials: Computational Aspects. *J. Phys. Chem. B* **2001**, *105* (31), 7375–7383.

(188) Akten, E. D.; Siriwardane, R.; Sholl, D. S. Monte Carlo Simulation of Single- and Binary-Component Adsorption of CO2, N2, and H2 in Zeolite Na-4A. *Energy & Fuels* **2003**, *17* (7), 977–983.

(189) Corma, A.; Garcia, H. Supramolecular Host-Guest Systems in Zeolites Prepared by Ship-in-a-Bottle Synthesis. *Eur. J. Inorg. Chem.* **2004**, 1143–1164.

(190) Ravoo, B. J. Nanofabrication with Metal Containing Dendrimers. *Dalton Trans.* **2008**, No. C, 1533–1537.

Table of Contents Entry

A Topological Analysis of Void Spaces in Tungstate Frameworks: Assessing Storage Properties for the Environmentally Important Guest Molecules and Ions: CO_2, UO_2, PuO_2, U, Pu, Sr^{2+}, Cs^+, CH_4, and H_2

By Jacqueline M. Cole, Alisha J. Cramer and Anita Zeidler

Synopsis: Topological analysis is employed to match the size and shape of voids (white) within tungstate host structures (blue) to that of environmentally important guest molecules, atoms or ions, which need a storage medium.